# Effects of railway track design on the expected degradation
## Parametric study on energy dissipation

Sadri, Mehran; Steenbergen, Michaël

**DOI**
10.1016/j.jsv.2018.01.029

**Publication date**
2018

**Document Version**
Accepted author manuscript

**Published in**
Journal of Sound and Vibration

**Citation (APA)**
Sadri, M., & Steenbergen, M. (2018). Effects of railway track design on the expected degradation: Parametric study on energy dissipation. *Journal of Sound and Vibration*, *419*, 281-301. https://doi.org/10.1016/j.jsv.2018.01.029

# Effects of railway track design on the expected degradation: parametric study on energy dissipation

Mehran Sadri and Michaël Steenbergen*

Delft University of Technology, Faculty of Civil Engineering and Geosciences, Railway Engineering Group, Stevinweg 1, 2628 CN Delft, The Netherlands

* Corresponding author,
Tel: +31 15 2783385; Email address: m.j.m.m.steenbergen@tudelft.nl

**Abstract**

This paper studies the effect of railway track design parameters on the expected long-term degradation of track geometry. The study assumes a geometrically perfect and straight track along with spatial invariability, except for the presence of discrete sleepers. A frequency-domain two-layer model is used of a discretely supported rail coupled with a moving unsprung mass. The susceptibility of the track to degradation is objectively quantified by calculating the mechanical energy dissipated in the substructure under a moving train axle for variations of different track parameters. Results show that, apart from the operational train speed, the ballast/substructure stiffness is the most significant parameter influencing energy dissipation. Generally, the degradation increases with the train speed and with softer substructures. However, stiff subgrades appear more sensitive to particular train velocities, in a regime which is mostly relevant for conventional trains (100-200 km/h) and less for high-speed operation, where a stiff subgrade is always favorable and can reduce the sensitivity to degradation substantially, with roughly a factor up to 7. Also railpad stiffness, sleeper distance and rail cross-sectional properties are found to have considerable effect, with higher expected degradation rates for increasing railpad stiffness, increasing sleeper distance and decreasing rail profile bending stiffness. Unsprung vehicle mass and sleeper mass have no significant influence, however, only against the background of the assumption of an idealized (invariant and straight) track. Apart from dissipated mechanical energy, the suitability of the dynamic track stiffness is explored as an engineering parameter to assess the sensitivity to degradation. It is found that this quantity is inappropriate to assess the design of an idealized track.

*Keywords*: Track degradation, Long-term track performance, Track settlement, Energy dissipation, Track design, Dynamic track stiffness.

## 1 Introduction and scope

Degradation of the railway substructure, in terms of settlements and the development of geometrical deviations of the track, has become a significant issue in recent years. Improving the long-term structural performance avoids the need of frequent inspection and maintenance and leads to an increased availability for railway tracks. In order to achieve such an improved long-term performance, it is essential to understand the relation between track degradation and track parameters. Such an understanding can be particularly relevant during the design stage of the track. Traditionally, railway track (and especially substructure) design is strongly focused on bearing capacity, and therefore on the instantaneous or short-term response. This means that the design is mostly purely static or quasistatic, without any proper consideration in the time domain, for example specifying the allowable track deflection under a given axle load [1]. Because degradation is a time-dependent process, induced by a loading process with a time history, such a design can never anticipate on degradation mechanisms and is therefore 'blind' for long-term developments. This can be illustrated also from the variables considered in track design: loading is expressed in terms of forces, and the structural response typically in terms of displacements, stresses and strains. These are variables apt to describe a 'status' in space and time. Degradation is however, in its most elementary form, always a mechanical energy dissipation process, described in terms of variables such as power and energy that account for variation in time.

Earlier studies in this field [2, 3] identified as a primary source of track degradation, apart from autonomous soil settlement, the occurrence of a dynamic component of the axle load. This component gives rise to a dynamic - and therefore highly efficient - compaction of the subgrade, leading to irregular track settlement [2]. Such a dynamic component may occur in principle due to three effects:

*i.* Wheel out-of-roundness (OOR) of the rolling stock, notably lower-order OOR leading to low-frequency dynamic wheel-track interaction [2];
*ii.* Longitudinal variability of the cross-sectional properties of the track itself - either periodic or non-periodic, leading to transition radiation in the track under moving axle loads [3];
*iii.* Track irregularity, notably the relatively short-wave defects in the loaded track geometry, which lead to the highest train-track interaction forces.

The existence of a dynamic axle load as a source of degradation has as its point of departure an existing track, at some point during its service life, with given parameters and train loading. The scope of this paper is situated on a different level. It addresses the effects of the track design itself, and more specifically of the elastic and inertial properties of its components and their spatial configuration, on the expected degradation rate. The point of departure in this first study into this subject is a straight and uniform track with no spatial variation except for that periodic one given by the discrete sleeper support, thereby purely considering the effects of track design choices.

The theoretical, qualitative and quantitative modelling of degradation, especially for granular and porous materials such as ballast and soil, is extremely complex and very sensitive to specific material properties [4, 5]. This is reflected in the empirical nature of many track degradation models describing long-term behavior of railway track, as found in the literature. Dahlberg [5] provides an overview of such empirical models. Sato [6] observed that track settlement could be divided into two phases and introduced two different mathematical expressions describing the short-term and long-term settlement, on the basis of curve-fitting. Using field data and a multivariable regression analysis, Lyngby [7] developed a model and investigated the effect of axle load and different types of track components (rail, sleeper, soil) on track degradation. Sadeghi and Askarinejad [8] examined the sensitivity of the track deterioration to structural and traffic parameters, by employing a track quality index derived from track geometry data. Varandas et al. [9] have employed an empirical model for the ballast settlement together with a train/track model in order to predict settlement of ballasted track specifically at transition zones. Abadi et al. [10] used measured data from the Southampton railway testing facility (SRTF) in order to evaluate the capability of different empirical ballast settlement models. They indicated that there is a significant difference between the results predicted by different previously-developed empirical models. Soleimanmeigouni et al. [11] reviewed and classified available models for track geometry degradation. Empirical models may help engineers to make a rough maintenance forecast of railway tracks; however, these models do not have a theoretical basis nor provide any fundamental insight. Moreover, only a limited number of parameters or factors have been taken into account for most of these empirical relationships. In order to avoid the difficulties inherent to a proper constitutive modelling of cohesive and non-cohesive granular materials involved in the track substructure, this study uses a different approach to get a grip on the complex issue of degradation. In line with the earlier study [3], it can be stated that dissipation of mechanical energy in a component or system is a precondition for - or even a most elementary representation of - its degradation. In other words, a conservative system is free of degradation. It is therefore sufficient to determine the effect of parametric variation of the properties of a mechanical system under time-dependent loading on localized energy dissipation in order to assess the susceptibility of the system to degradation of specific components.

The first step in the investigation therefore comprises the development of a model for short-term dynamic analysis of the track, capable to describe the mechanical energy flux of relevant individual track components during the loading process. A second step consists in the parametric evaluation of this model with respect to dissipated energy. Energy dissipation, although a very suitable quantity for theoretical analysis, is in itself also a rather abstract quantity which cannot be measured in the field. In practice, often a different engineering parameter is employed: the dynamic track stiffness. This is a measurable quantity for which good results have been obtained in practice and reported in the literature over the past years, in the sense that dynamic track stiffness variations correlate with degradation hotspots. This fact is at the

basis of the development of e.g. the Swedish rolling stiffness measurement vehicle. Berggren et al. [12, 13] analyzed dynamic track stiffness measured along the track and indicated that variations of track stiffness significantly affect the degradation rate of the track. Variation of track stiffness within a short distance and its effect on track settlement have been discussed in [14]. Identification of substructure properties using measured dynamic stiffness of the track was carried out in [15, 16]. Using an experimental approach, Luomala and Nurmikolu [17] studied the effect of maintenance on the track stiffness measured at bridge transition zones. Although not theoretically derived or proven, an empirical relationship between stiffness variation and degradation makes physically sense. The dynamic track stiffness is the resistance against deflection experienced in the wheel-rail contact by the moving axle load. Variation of this experienced resistance therefore leads to a variation in the structural response moving along with the load, and therefore to a variation of the mechanical energy contained in this response. It can be expected that this energy flux is at least partially dissipated in the structure, localized at those positions where an energy excess occurs. In practice, such a measured stiffness variation accounts for non-uniformity of the track cross-sectional properties, whereas in this study a uniform track is assumed except for the sleeper periodicity. Nonetheless, the same physical reasoning can be applied to periodical non-uniformity. Therefore, this paper 'tests', in a third step, the applicability of the dynamic stiffness in order to describe the sensitivity of the degradation rate to parametric design choices. The theoretical definition of this dynamic track stiffness is further elaborated in paragraph 2.2.3.

Concerning the first step of the analysis mentioned before, many different track models have been proposed by researchers in order to study different aspects of track dynamics. They can be divided into two categories: analytical-numerical frequency-domain models and different types of time-domain models. The first type of models is computationally efficient and provides better insight into the system response. It is therefore very apt for parametric analyses aiming at fundamental understanding. Frequency-domain models have been applied in the past with different degrees of complexity and with different aims, ranging from very simple beam-on-elastic-foundation (BOEF) models [18-22] to more sophisticated two- or three-layer linear beam models accounting for discrete sleeper spacing and transient loading [23-28] and finally fully three-dimensional beam or plate on halfspace models (eventually with stratification), the latter ones with the aim of predicting environmental vibration due to moving trains [29-34]. Given the scope of the present study and its preliminary character, it is chosen to adopt a model that is on one hand no more complicated than strictly necessary, on the other hand able to describe all individual track components and take into account energy dissipation in the substructure or subsoil. Therefore, this individual sleeper support is represented by discrete Kelvin-Voigt elements. Although this representation can describe both the elastic resistance and the damping offered by the ballast and the soil supporting the sleeper when loaded by a train passing axle, it is certainly not the most appropriate one to quantify the damping/dissipation in the subgrade in an accurate way. However, given the aim of this work, to study the

effect of parametric variation on the dissipated energy as such, and to draw relative conclusions, it is sufficient. Moreover, it allows for an approach in the frequency domain. A second consideration is that increasing subgrade model complexity may easily suggest an accuracy which is only fictitious. As has been mentioned, the interaction between the discrete sleeper, the ballast layer and the deeper soil is extremely difficult to model; the very few constitutive ballast models that exist (such as [35]) show both an enormous bandwidth and a very high degree of non-linearity. Using a basic description while accounting for elementary features is, against this background, not necessarily a bad choice for obtaining comparative results. On the other hand, the adopted representation implies a limitation of the train speed in the model to subcritical velocities, because only for these velocities the eigenfield (surface displacement field) moving along with the axle load is confined to its immediate environment and there is no energy radiation. The rail itself is modeled using both Euler-Bernoulli and Timoshenko theory. Further, with respect to the train, the unsprung vehicle mass is included in the model, coupled to the track by the wheel-rail contact stiffness.

The main contribution of the present work, with respect to the state of the art in the modeling of track degradation, is the systematic assessment of the role of different track design parameters with respect to the susceptibility to substructure degradation. In this sense, it can be considered as a dynamic 'benchmarking' of traditional track design, with respect to its expected long-term performance. The assessment is relative and not quantitative. Therefore, the work does not allow for a quantification of degradation itself, for a given design at any moment during the service life. In order to do so, the cyclic loading process itself should be taken into account, along with the cyclic energy dissipation resulting into the development of the geometry in terms of ongoing settlements. This would involve the incorporation of the already discussed mechanism (*iii*) and the associated dynamic axle load, which is outside the scope of the present work.

The outline of this paper is as follows. Section 2 contains the mathematical framework of the study, in terms of formulations employed for dynamic modeling of the wheel/track system and expressions for both the energy dissipated in the substructure and the dynamic track stiffness. Section 3 presents results from a parametric study, in line with a discussion on the influence of track design on the energy dissipated in the substructure and the use of engineering parameters to assess long-term behavior. Section 4 closes with conclusions.

## 2 Theoretical framework

In the first part of this section, a frequency-domain model is developed for dynamic analysis of a discretely supported rail subjected to a moving wheel mass. Analytical closed-form expressions for the

energy dissipated in the substructure and the static and dynamic track stiffness are derived in the second part.

*2.1 A frequency-domain model for wheel/track dynamics*

As has been discussed in the introduction, a two-layer track model is adopted, and subjected to loading by a moving wheel mass. The two-layer track model is composed of a rail, modelled as an infinite Timoshenko beam, railpads as Kelvin-Voight elements, sleepers as rigid masses, and discrete sleeper supports by ballast and subsoil again as Kelvin-Voight elements. The moving wheel mass is coupled to the track through a contact spring, representing a linearised Hertzian contact, $k_H$. A schematic overview of the model is shown in Fig. 1. It is assumed in this study that the discrete supports are identical and the track model is therefore periodic. Since the model is periodic, an analytical approach can be employed, based on expressing the periodic response of the track and train-track interaction force as Fourier series.

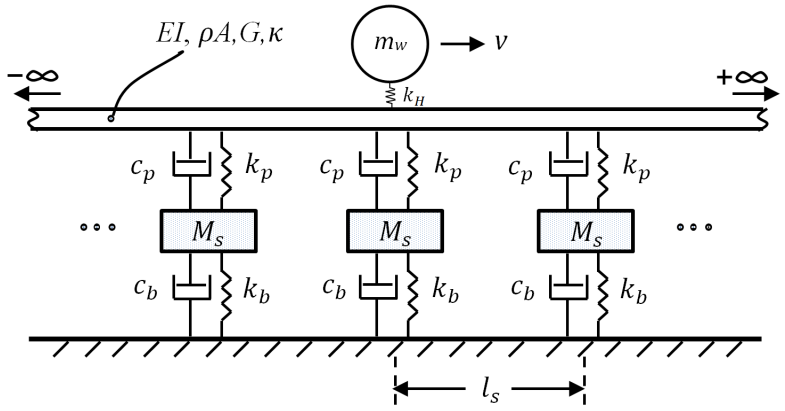


Fig. 1. A schematic of the mathematical model of the railway track subjected to a moving wheel mass

For the track model shown in Fig. 1, $EI, G$ and $\rho A$ denote the bending stiffness, shear modulus and mass per unit length of the rail, respectively; $\kappa$ the Timoshenko shear coefficient of the cross section of the rail beam; $M_s$ the sleeper mass; $k_p$ and $c_p$ the stiffness and the damping of the railpads; $k_b$ and $c_b$ the stiffness and the damping of the ballast/substructure; $l_s$ the sleeper distance; $m_w$ the unsprung wheel mass, and $v$ the train speed. As mentioned, the track is coupled to the moving wheel through a linear contact spring. The equation of the motion of the moving wheel can now be written as follows:

$$m_w \ddot{w}_w(t) = k_H \left( w_b(vt,t) - w_w(t) \right) + m_{tot} g, \tag{1}$$

where $m_{tot} g$ is half the axle load, $w_w(t)$ is the wheel displacement and $w_b(vt,t)$ denotes the rail displacement at the wheel-rail contact point. By employing the Timoshenko beam theory and considering $N_s + 1$ supports along the model, the equations of motion for the rail can be written as:

$$\rho A\frac{\partial^2 w_{\mathrm{b}}(x,t)}{\partial t^2}-\kappa AG\frac{\partial^2 w_{\mathrm{b}}(x,t)}{\partial x^2}+\kappa AG\frac{\partial \psi_{\mathrm{b}}(x,t)}{\partial x}=-F_{\mathrm{c}}(t)\delta(x-vt)-\sum_{i=-N_{\mathrm{s}}/2}^{N_{\mathrm{s}}/2}R_0(t-\frac{il_{\mathrm{s}}}{v})\delta(x-il_{\mathrm{s}}), \tag{2}$$

$$\rho I\frac{\partial^2 \psi_{\mathrm{b}}(x,t)}{\partial t^2}-EI\frac{\partial^2 \psi_{\mathrm{b}}(x,t)}{\partial x^2}-\kappa AG\frac{\partial w_{\mathrm{b}}(x,t)}{\partial x}+\kappa AG\psi_{\mathrm{b}}(x,t)=0, \tag{3}$$

in which $\delta(.)$ represents the Dirac-delta function and $F_{\mathrm{c}}(t)$ and $R_0(t)$ are defined in the following equations:

$$F_{\mathrm{c}}(t)=k_{\mathrm{H}}\left(w_{\mathrm{b}}(vt,t)-w_{\mathrm{w}}(t)\right), \tag{4}$$

$$R_0(t)=k_{\mathrm{p}}\{w_{\mathrm{b}}(0,t)-w_{\mathrm{s},0}(t)\}+c_{\mathrm{p}}\{\dot{w}_{\mathrm{b}}(0,t)-\dot{w}_{\mathrm{s},0}(t)\}, \tag{5}$$

where $w_{\mathrm{s},0}(t)$ is the displacement of the sleeper at $x=0$. Taking into account the interaction force between the rail and the sleeper at $x=0$ defined in Eq. (5), the equation of the motion for this sleeper is given as:

$$M_{\mathrm{s}}\ddot{w}_{\mathrm{s},0}(t)=R_0(t)-c_{\mathrm{b}}\dot{w}_{\mathrm{s},0}(t)-k_{\mathrm{b}}w_{\mathrm{s},0}(t). \tag{6}$$

As mentioned, it is assumed that the discrete supports in the model are identical and the model is periodic. Consequently, the following relationship can be established between the reaction force of the *i*th support and the reaction force of the support at $x=0$, i.e. $R_i(t)$ and $R_0(t)$:

$$R_i(t)=R_0(t-\frac{il_s}{v}). \tag{7}$$

Since the model is assumed to be periodic with the period equal to $l_{\mathrm{s}}/v$, the displacement and the rotation angle of the cross-section of the rail, the displacement of the moving wheel and the wheel-rail contact force satisfy the following equations:

$$\begin{cases} w_{\mathrm{b}}(x+l_{\mathrm{s}},t+\frac{l_{\mathrm{s}}}{v})=w_{\mathrm{b}}(x,t) \\ \psi_{\mathrm{b}}(x+l_{\mathrm{s}},t+\frac{l_{\mathrm{s}}}{v})=\psi_{\mathrm{b}}(x,t) \\ w_{\mathrm{w}}(t+\frac{l_{\mathrm{s}}}{v})=w_{\mathrm{w}}(t) \\ F_{\mathrm{c}}(t+\frac{l_{\mathrm{s}}}{v})=F_{\mathrm{c}}(t) \end{cases}. \tag{8}$$

Therefore, the contact force can be expressed as a Fourier series and the following equation can be written:

$$F_{\mathrm{c}}(t)=\sum_{m=-\infty}^{+\infty}\overline{F}_m\,\mathrm{e}^{\mathrm{j}m(\frac{2\pi v}{l_{\mathrm{s}}})t}, \tag{9}$$

where $\mathrm{j}^2=-1$ and $\overline{F}_m$ are the unknown coefficients of the contact force. Furthermore, Eq. (8) can be utilized in order to find the following relationships for the Fourier transform of the beam displacement and rotation:

$$\hat{w}_{\mathrm{b}}(x,\omega)=\int_{-\infty}^{+\infty} w_{\mathrm{b}}(x+l_{\mathrm{s}},t+\frac{l_{\mathrm{s}}}{v})\mathrm{e}^{-\mathrm{j}\omega t}\mathrm{d}t=\mathrm{e}^{\mathrm{j}\omega l_{\mathrm{s}}/v}\hat{w}_{\mathrm{b}}(x+l_{\mathrm{s}},\omega). \tag{10}$$

$$\hat{\psi}_{\mathrm{b}}(x,\omega)=\mathrm{e}^{\mathrm{j}\omega l_{\mathrm{s}}/v}\hat{\psi}_{\mathrm{b}}(x+l_{\mathrm{s}},\omega). \tag{11}$$

It can be concluded from the latter relationships that the Fourier transform of the displacement and rotation of the infinite beam are spatially periodic and they can therefore be expressed using the following Fourier series:

$$\hat{w}_{\mathrm{b}}(x,\omega)=\mathrm{e}^{-\mathrm{j}\omega x/v}\sum_{m=-\infty}^{+\infty}\bar{W}_m(\omega)\mathrm{e}^{\mathrm{j}m(\frac{2\pi}{l_{\mathrm{s}}})x}, \tag{12}$$

$$\hat{\psi}_{\mathrm{b}}(x,\omega)=\mathrm{e}^{-\mathrm{j}\omega x/v}\sum_{m=-\infty}^{+\infty}\bar{\psi}_m(\omega)\mathrm{e}^{\mathrm{j}m(\frac{2\pi}{l_{\mathrm{s}}})x}, \tag{13}$$

where $\bar{W}_m(\omega)$ and $\bar{\psi}_m(\omega)$ are the unknown frequency-dependent coefficients of the displacement and rotation responses. It is worth noting that the beam displacement and rotation responses given in Eqs. (12) and (13) satisfy the periodicity conditions introduced in Eqs. (10) and (11). One can now take the Fourier transform of the both sides of Eqs. (2) and (3) with respect to time, use Eq. (9) and obtain the following equations:

$$-\rho A\omega^2\hat{w}_{\mathrm{b}}(x,\omega)-\kappa AG\frac{\partial^2\hat{w}_{\mathrm{b}}(x,\omega)}{\partial x^2}+\kappa AG\frac{\partial\hat{\psi}_{\mathrm{b}}(x,\omega)}{\partial x}=-\int_{-\infty}^{+\infty}\sum_{m=-\infty}^{+\infty}\bar{F}_m\mathrm{e}^{\mathrm{j}m(\frac{2\pi v}{l_{\mathrm{s}}})t}\delta(x-vt)\mathrm{e}^{-\mathrm{j}\omega t}dt$$
$$-\int_{-\infty}^{+\infty}\sum_{i=-N_{\mathrm{s}}/2}^{N_{\mathrm{s}}/2}R_0(t-\frac{il_{\mathrm{s}}}{v})\delta(x-il_{\mathrm{s}})\mathrm{e}^{-\mathrm{j}\omega t}dt, \tag{14}$$

$$-\rho I\omega^2\hat{\psi}_{\mathrm{b}}(x,\omega)-EI\frac{\partial^2\hat{\psi}_{\mathrm{b}}(x,\omega)}{\partial x^2}-\kappa AG\frac{\partial\hat{w}_{\mathrm{b}}(x,\omega)}{\partial x}+\kappa AG\hat{\psi}_{\mathrm{b}}(x,\omega)=0, \tag{15}$$

where $\hat{R}_0(\omega)$ is the Fourier transform of $R_0(t)$. The Fourier representations of the responses given in Eqs. (12) and (13) as well as their derivatives can be substituted into the latter equations in order to find the following relationship between the unknown coefficients of the displacement and rotation of the beam:

$$\bar{\psi}_m(\omega)=\Pi_m^*(\omega)\bar{W}_m(\omega), \tag{16}$$

where $\Pi_m^*(\omega)$ is defined below:

$$\Pi_m^*(\omega)=\frac{\mathrm{j}\left(\frac{2\pi m}{l_s}-\frac{\omega}{v}\right)\kappa AG}{EI\left(\frac{2\pi m}{l_s}-\frac{\omega}{v}\right)^2+\kappa AG-\rho I\omega^2}. \tag{17}$$

Moreover, in order to be able to find the unknown coefficients of the beam displacement in terms of the contact force coefficients (from Eq. (14)), the reaction force of the support at $x=0$ in the frequency

domain, i.e. $\hat{R}_0(\omega)$, must also be found and substituted into Eq. (14). Taking the Fourier transform of Eq. (5) with respect to time yields:

$$\hat{R}_0(\omega) = \left(\mathrm{j}\omega c_\mathrm{p} + k_\mathrm{p}\right)\left(\hat{w}_\mathrm{b}(0,\omega) - \hat{w}_{\mathrm{s},0}(\omega)\right). \tag{18}$$

The displacement of the sleeper at $x = 0$ in the frequency domain, i.e. $\hat{w}_{\mathrm{s},0}(\omega)$, can be found by combining the latter equation with the Fourier transform of Eq. (6):

$$\hat{w}_{\mathrm{s},0}(\omega) = \frac{\mathrm{j}\omega c_\mathrm{p} + k_\mathrm{p}}{-\omega^2 M_\mathrm{s} + \mathrm{j}\omega(c_\mathrm{p} + c_\mathrm{b}) + (k_\mathrm{p} + k_\mathrm{b})}\hat{w}_\mathrm{b}(0,\omega), \tag{19}$$

and subsequently, the reaction force can be obtained by substituting Eq. (19) into Eq. (18):

$$\hat{R}_0(\omega) = \left[\frac{\left(\mathrm{j}\omega c_\mathrm{p} + k_\mathrm{p}\right)\left(-\omega^2 M_\mathrm{s} + \mathrm{j}\omega c_\mathrm{b} + k_\mathrm{b}\right)}{-\omega^2 M_\mathrm{s} + \mathrm{j}\omega(c_\mathrm{p} + c_\mathrm{b}) + (k_\mathrm{p} + k_\mathrm{b})}\right]\hat{w}_\mathrm{b}(0,\omega). \tag{20}$$

Finally, the reaction force of the support at $x = 0$ can be expressed in terms of the unknown coefficients of the beam displacement; this can be carried out by utilizing Eq. (20) together with the frequency response defined in Eq. (12):

$$\hat{R}_0(\omega) = \sum_{m=-\infty}^{+\infty} G(\omega)\overline{W}_m(\omega), \tag{21}$$

where $G(\omega)$ is defined in the following equation:

$$G(\omega) = \frac{\left(\mathrm{j}\omega c_\mathrm{p} + k_\mathrm{p}\right)\left(-\omega^2 M_\mathrm{s} + \mathrm{j}\omega c_\mathrm{b} + k_\mathrm{b}\right)}{-\omega^2 M_\mathrm{s} + \mathrm{j}\omega(c_\mathrm{p} + c_\mathrm{b}) + (k_\mathrm{p} + k_\mathrm{b})}. \tag{22}$$

Employing Eqs. (12), (13) and (16), it is possible to rewrite Eq. (14):

$$\begin{aligned}&\sum_{m=-\infty}^{+\infty}\left\{\overline{W}_m(\omega)\mathrm{e}^{\mathrm{j}\left(\frac{2\pi m}{l_\mathrm{s}} - \frac{\omega}{v}\right)x}\left(\kappa AG\left[\frac{2\pi m}{l_\mathrm{s}} - \frac{\omega}{v}\right]^2 + \kappa AG.\,\mathrm{j}\left[\frac{2\pi m}{l_\mathrm{s}} - \frac{\omega}{v}\right]\Pi_m^*(\omega) - \rho A\omega^2\right) + \frac{\overline{F}_m}{v}\mathrm{e}^{\mathrm{j}\left(\frac{2\pi m}{l_\mathrm{s}} - \frac{\omega}{v}\right)x}\right\} = \\ &= -\sum_{i=-N_\mathrm{s}/2}^{N_\mathrm{s}/2}\hat{R}_0(\omega)\delta(x - il_\mathrm{s})\mathrm{e}^{-\mathrm{j}\omega(il_\mathrm{s}/v)}.\end{aligned} \tag{23}$$

The reaction force given in Eq. (21) can now be substituted into Eq. (23) and the following equation can be derived:

$$\sum_{m=-\infty}^{+\infty}\left\{\overline{W}_m(\omega)\left[\Lambda^*_{m,\mathrm{Timoshenko}}(\omega)\mathrm{e}^{\mathrm{j}\left(\frac{2\pi m}{l_\mathrm{s}} - \frac{\omega}{v}\right)x} + \sum_{i=-\infty}^{+\infty}\delta(x - il_\mathrm{s})G(\omega)\mathrm{e}^{-\mathrm{j}\left(\frac{il_\mathrm{s}}{v}\right)\omega}\right] + \frac{1}{v}\overline{F}_m\mathrm{e}^{\mathrm{j}\left(\frac{2\pi m}{l_\mathrm{s}} - \frac{\omega}{v}\right)x}\right\} = 0, \tag{24}$$

where $\Lambda^*_{m,\mathrm{Timoshenko}}(\omega)$ is defined as:

$$\Lambda^{*}_{m,\text{Timoshenko}}(\omega)=\kappa AG\left[\frac{2\pi m}{l_{\text{s}}}-\frac{\omega}{v}\right]^{2}+\text{j}\left[\frac{2\pi m}{l_{\text{s}}}-\frac{\omega}{v}\right]\kappa AG\,\Pi^{*}_{m}(\omega)-\rho A\omega^{2}. \tag{25}$$

Both the Euler and the Timoshenko beam theories are implemented in this paper for comparison. An equation relating the unknown coefficients of the beam displacement to the unknown coefficients of the contact force was already derived for the Timoshenko model (see Eq. (24)). The same procedure can be followed and a similar equation can be found for the Euler model. In fact, to be able to use Eq. (24) for the Euler beam, one needs to replace $\Lambda^{*}_{m,\text{Timoshenko}}(\omega)$ in this equation with $\Lambda^{*}_{m,\text{Euler}}(\omega)$ defined in the following equation:

$$\Lambda^{*}_{m,\text{Euler}}(\omega)=EI\left[\frac{2\pi m}{l_{\text{s}}}-\frac{\omega}{v}\right]^{4}-\rho A\omega^{2}. \tag{26}$$

In the rest of the section, to provide a general formulation including both the beam theories, we will use $\Lambda_{m}(\omega)$, which is defined as $\Lambda^{*}_{m,\text{Timoshenko}}(\omega)$ and $\Lambda^{*}_{m,\text{Euler}}(\omega)$ for the Timoshenko and Euler beams, respectively. Using the sampling property of the Dirac comb as well as its periodicity, Eq. (24) can be rewritten as:

$$\sum_{m=-\infty}^{+\infty}\left\{\overline{W}_{m}(\omega)\left[\text{e}^{\text{j}(\frac{2\pi m}{l_{\text{s}}}-\frac{\omega}{v})x}\Lambda_{m}(\omega)+\frac{1}{l_{\text{s}}}G(\omega)\text{e}^{-\text{j}(\frac{\omega}{v})x}\sum_{n=-\infty}^{+\infty}\text{e}^{\text{j}(\frac{2\pi n}{l_{\text{s}}})x}\right]+\frac{1}{v}\overline{F}_{m}\text{e}^{\text{j}(\frac{2\pi m}{l_{\text{s}}}-\frac{\omega}{v})x}\right\}=0. \tag{27}$$

By eliminating $\text{e}^{-\text{j}(\frac{\omega}{v})x}$ from Eq. (27), it takes the following form:

$$\sum_{m=-\infty}^{+\infty}\left\{\overline{W}_{m}(\omega)\left[\Lambda_{m}(\omega)\text{e}^{\text{j}(\frac{2\pi m}{l_{\text{s}}})x}+\frac{1}{l_{\text{s}}}G(\omega)\sum_{n=-\infty}^{+\infty}\text{e}^{\text{j}(\frac{2\pi n}{l_{\text{s}}})x}\right]+\frac{1}{v}\overline{F}_{m}\text{e}^{\text{j}(\frac{2\pi m}{l_{\text{s}}})x}\right\}=0. \tag{28}$$

By truncating the latter equation and considering $2N_{\text{t}}+1$ terms of the infinite series ($m=-N_{\text{t}},...,N_{\text{t}}$), and using linear independence of the exponential functions, the following equation in matrix form can be introduced:

$$\mathbf{CO}_{(2N_{\text{t}}+1)\times(2N_{\text{t}}+1)}\,\overline{\mathbf{W}}_{(2N_{\text{t}}+1)\times 1}=-\frac{1}{v}\overline{\mathbf{F}}_{(2N_{\text{t}}+1)\times 1}, \tag{29}$$

where $\mathbf{CO}$, $\overline{\mathbf{W}}$ and $\overline{\mathbf{F}}$ are given as follows:

$$\mathbf{CO}=\begin{bmatrix} \Lambda_{-N_t}(\omega)+\dfrac{G(\omega)}{l_s} & \dfrac{G(\omega)}{l_s} & \dfrac{G(\omega)}{l_s} & \cdots & \dfrac{G(\omega)}{l_s} \\ \dfrac{G(\omega)}{l_s} & \Lambda_{-N_t+1}(\omega)+\dfrac{G(\omega)}{l_s} & \dfrac{G(\omega)}{l_s} & \cdots & \dfrac{G(\omega)}{l_s} \\ \vdots & \vdots & \vdots & \ddots & \vdots \\ \dfrac{G(\omega)}{l_s} & \dfrac{G(\omega)}{l_s} & \cdots & \dfrac{G(\omega)}{l_s} & \Lambda_{N_t}(\omega)+\dfrac{G(\omega)}{l_s} \end{bmatrix}, \overline{\mathbf{W}}=\begin{Bmatrix} \overline{W}_{-N_t}(\omega) \\ \overline{W}_{-N_t+1}(\omega) \\ \vdots \\ \overline{W}_0(\omega) \\ \overline{W}_1(\omega) \\ \vdots \\ \overline{W}_{N_t}(\omega) \end{Bmatrix}, \quad \overline{\mathbf{F}}=\begin{Bmatrix} \overline{F}_{-N_t} \\ \overline{F}_{-N_t+1} \\ \vdots \\ \overline{F}_0 \\ \overline{F}_1 \\ \vdots \\ \overline{F}_{N_t} \end{Bmatrix}. \tag{30}$$

Now, if we define $\boldsymbol{\Theta}$ as the inverse of $\mathbf{CO}$, i.e. $\boldsymbol{\Theta}=\mathbf{CO}^{-1}$, the unknown coefficients of the beam displacement can be found in terms of the contact force coefficients and elements of $\boldsymbol{\Theta}$:

$$\overline{W}_m(\omega)=-\frac{1}{v}\sum_{n=-N_t}^{N_t}\Theta_{m+(N_t+1),n+(N_t+1)}\overline{F}_n, \quad m=-N_t,...,N_t, \tag{31}$$

where $\Theta_{i,j}$ is the *(i,j)*th element of $\boldsymbol{\Theta}$. Substituting Eq. (31) into (12) yields:

$$\hat{w}_b(x,\omega)=-\frac{1}{v}e^{-j\omega x/v}\sum_{m=-N_t}^{N_t}\sum_{n=-N_t}^{N_t}\Theta_{m+(N_t+1),n+(N_t+1)}\overline{F}_n e^{jm(\frac{2\pi}{l_s})x}. \tag{32}$$

$w_b(x,t)$, i.e. the response of the beam in time domain, can be obtained from the latter equation by taking the inverse Fourier transform with respect to $\omega$:

$$w_b(x,t)=-\frac{1}{v}\sum_{m=-N_t}^{N_t}\sum_{n=-N_t}^{N_t}(\theta(t-\frac{x}{v}))_{m+(N_t+1),n+(N_t+1)}\overline{F}_n e^{jm(\frac{2\pi}{l_s})x}, \tag{33}$$

where $(\theta(t))_{i,j}$ is defined as follow:

$$(\theta(t))_{i,j}=\frac{1}{2\pi}\int_{-\infty}^{+\infty}\Theta_{i,j}e^{j\omega t}d\omega. \tag{34}$$

Utilizing Eqs. (4), (9) and (33), the displacement of the moving wheel can be obtained in terms of the contact force coefficients:

$$w_w(t)=-\sum_{m=-N_t}^{N_t}\left\{\frac{\overline{F}_m}{k_H}+\frac{1}{v}\sum_{n=-N_t}^{N_t}(\theta(0))_{m+(N_t+1),n+(N_t+1)}\overline{F}_n\right\}e^{jm(\frac{2\pi v}{l_s})t}. \tag{35}$$

Both the response of the infinite beam and the moving wheel have been found as a function of the contact force (see Eqs. (33) and (35)). Therefore, these responses can be substituted into Eq. (1) in order to establish the following set of algebraic equations:

$$m_w\left(\frac{2\pi mv}{l_s}\right)^2\left\{\frac{\overline{F}_m}{k_H}+\frac{1}{v}\sum_{n=-N_t}^{N_t}(\theta(0))_{m+(N_t+1),n+(N_t+1)}\overline{F}_n\right\}=\overline{F}_m, \ m=-N_t,...,N_t, \ m\neq 0. \tag{36}$$

It should be noted that the contact force coefficient corresponding to $m=0$ is equal to the static wheel load, i.e. $\overline{F}_0 = -m_{\text{tot}} g$ . Eq. (36) can be written in a matrix form:

$$\boldsymbol{\varphi}_{2N_t \times 2N_t} \overline{\mathbf{f}}_{2N_t \times 1} = \frac{-\overline{F}_0}{v} \boldsymbol{\theta}^*_{2N_t \times 1}, \tag{37}$$

where $\boldsymbol{\varphi}$, $\overline{\mathbf{f}}$ and $\boldsymbol{\theta}^*$ are given below:

$$\boldsymbol{\varphi} = \begin{bmatrix} \varphi_{1,1} & \varphi_{1,2} & \cdots & \varphi_{1,N_t} & \varphi_{1,N_t+2} & \varphi_{1,N_t+3} & \cdots & \varphi_{1,2N_t+1} \\ \varphi_{2,1} & \varphi_{2,2} & \cdots & \varphi_{2,N_t} & \varphi_{2,N_t+2} & \varphi_{2,N_t+3} & \cdots & \varphi_{2,2N_t+1} \\ \vdots & \vdots & \ddots & \vdots & \vdots & \vdots & \vdots & \vdots \\ \varphi_{N_t,1} & \varphi_{N_t,2} & \cdots & \varphi_{N_t,N_t} & \varphi_{N_t,N_t+2} & \varphi_{N_t,N_t+3} & \cdots & \varphi_{N_t,2N_t+1} \\ \varphi_{N_t+2,1} & \varphi_{N_t+2,2} & \cdots & \varphi_{N_t+2,N_t} & \varphi_{N_t+2,N_t+2} & \varphi_{N_t+2,N_t+3} & \cdots & \varphi_{N_t+2,2N_t+1} \\ \varphi_{N_t+3,1} & \varphi_{N_t+3,2} & \cdots & \varphi_{N_t+3,N_t} & \varphi_{N_t+3,N_t+2} & \varphi_{N_t+3,N_t+3} & \cdots & \varphi_{N_t+3,2N_t+1} \\ \vdots & \vdots & \vdots & \vdots & \vdots & \vdots & \ddots & \vdots \\ \varphi_{2N_t+1,1} & \varphi_{2N_t+1,2} & \cdots & \varphi_{2N_t+1,N_t} & \varphi_{2N_t+1,N_t+2} & \varphi_{2N_t+1,N_t+3} & \cdots & \varphi_{2N_t+1,2N_t+1} \end{bmatrix}, \tag{38}$$

$$\overline{\mathbf{f}} = \begin{bmatrix} \overline{F}_{-N_t} \\ \overline{F}_{-N_t+1} \\ \vdots \\ \overline{F}_{-1} \\ \overline{F}_1 \\ \overline{F}_2 \\ \vdots \\ \overline{F}_{N_t} \end{bmatrix}, \quad \boldsymbol{\theta}^* = \begin{bmatrix} (\theta(0))_{1,N_t+1} \\ (\theta(0))_{2,N_t+1} \\ \vdots \\ (\theta(0))_{N_t,N_t+1} \\ (\theta(0))_{N_t+2,N_t+1} \\ (\theta(0))_{N_t+3,N_t+1} \\ \vdots \\ (\theta(0))_{2N_t+1,N_t+1} \end{bmatrix}. \tag{39}$$

The elements of $\boldsymbol{\varphi}$ in Eq. (38) are calculated from the following equation:

$$\begin{cases} \varphi_{i,j} = \dfrac{1}{k_{\text{H}}} - \dfrac{l_{\text{s}}^{\,2}}{m_{\text{w}}(2\pi v(i-N_{\text{t}}-1))^2} + \dfrac{(\theta(0))_{i,j}}{v} & \text{if } i = j \\ \varphi_{i,j} = \dfrac{(\theta(0))_{i,j}}{v} & \text{if } i \neq j \end{cases}. \tag{40}$$

Finally, the unknown coefficients of the wheel-rail contact force can be found from Eq. (37):

$$\overline{\mathbf{f}}_{2N_t \times 1} = \frac{-\overline{F}_0}{v} \boldsymbol{\varphi}^{-I}_{2N_t \times 2N_t} \boldsymbol{\theta}^*_{2N_t \times 1}. \tag{41}$$

As soon as the unknown coefficients of the contact force are found, the dynamic response of the beam and the moving wheel can be obtained from Eq. (33) and (35), respectively.

*2.2 Parameters for assessment of long-term performance*

As has been discussed in Section 1, this study first considers mechanical energy dissipation in the substructure, represented by Kelvin-Voight elements under the individual sleepers, as a measure for evaluating long-term performance of railway track in service. As an engineering parameter, dynamic track stiffness variation was adopted. This quantity will be considered relative to the static track stiffness, which is therefore derived as well.

*2.2.1 Mechanical energy dissipation in the substructure*

The velocity response of the sleeper at $x = 0$ in the frequency-domain can be obtained using the frequency response in Eq. (19):

$$\hat{v}_{\mathrm{s},0}(\omega) = \mathrm{j}\omega\hat{w}_{\mathrm{s},0}(\omega) = \frac{\mathrm{j}\omega\left(\mathrm{j}\omega c_{\mathrm{p}} + k_{\mathrm{p}}\right)}{-\omega^2 M_{\mathrm{s}} + \mathrm{j}\omega(c_{\mathrm{p}} + c_{\mathrm{b}}) + (k_{\mathrm{p}} + k_{\mathrm{b}})}\hat{w}_{\mathrm{b}}(0,\omega), \tag{42}$$

where the frequency response of the beam at $x = 0$, i.e. $\hat{w}_{\mathrm{b}}(0,\omega)$, is given in Eq. (32). For one passage of the moving wheel, the energy dissipated by the substructure/ballast damping in the support located at $x = 0$ is calculated as:

$$E_{\mathrm{diss},0} = \int_{-\infty}^{+\infty} F_{\mathrm{c},0}(t) v_{\mathrm{s},0}(t)\,dt = \int_{-\infty}^{+\infty} c_{\mathrm{b}} v_{\mathrm{s},0}(t)^2\,dt, \tag{43}$$

in which $v_{\mathrm{s},0}(t)$ is the velocity response of the sleeper at $x = 0$ in the time domain, and can be obtained by taking the inverse Fourier transform of Eq. (42).

*2.2.2 The static track stiffness*

Differential equations governing the static response of a discretely supported Timoshenko beam under a static load (at $x = x_{\mathrm{F}}$) are given as:

$$\kappa AG\frac{\partial\psi_{\mathrm{b}}(x)}{\partial x} - \kappa AG\frac{\partial^2 w_{\mathrm{b}}(x)}{\partial x^2} = F_0\delta(x - x_{\mathrm{F}}) - \sum_{i=-N_{\mathrm{s}}/2}^{N_{\mathrm{s}}/2} k_{\mathrm{p}}\left(w_{\mathrm{b}}(il_{\mathrm{s}}) - w_{\mathrm{s},i}\right)\delta(x - il_{\mathrm{s}}), \tag{44}$$

$$-EI\frac{\partial^2\psi_{\mathrm{b}}(x)}{\partial x^2} - \kappa AG\frac{\partial w_{\mathrm{b}}(x)}{\partial x} + \kappa AG\psi_{\mathrm{b}}(x) = 0. \tag{45}$$

The static deflection of the *i*th sleeper, i.e. $w_{\mathrm{s},i}$, can be found from its static equilibrium equation:

$$w_{\mathrm{s},i} = \left( \frac{k_\mathrm{p}}{k_\mathrm{p} + k_\mathrm{b}} \right) w_\mathrm{b}(il_\mathrm{s}). \tag{46}$$

One can now Substitute Eq. (46) into Eq. (44), take a Fourier transform with respect to *x* and derive the following equation:

$$\kappa AG\xi^2 \hat{w}_\mathrm{b}(\xi) + \mathrm{j}\xi\kappa AG\hat{\psi}_\mathrm{b}(\xi) = F_0 \mathrm{e}^{-\mathrm{j}\xi x_\mathrm{F}} - \sum_{i=-N_\mathrm{s}/2}^{N_\mathrm{s}/2} \left( \frac{k_\mathrm{p} k_\mathrm{b}}{k_\mathrm{p} + k_\mathrm{b}} \right) w_\mathrm{b}(il_\mathrm{s}) \mathrm{e}^{-\mathrm{j}\xi il_\mathrm{s}}. \tag{47}$$

Furthermore, $\hat{\psi}_\mathrm{b}(\xi)$ can be found from the Fourier transformation of Eq. (45):

$$\hat{\psi}_\mathrm{b}(\xi) = \left( \frac{\mathrm{j}\xi\kappa AG}{EI\xi^2 + \kappa AG} \right) \hat{w}_\mathrm{b}(\xi). \tag{48}$$

The latter equation is substituted into Eq. (47) and the inverse Fourier transform is then applied in order to obtain the following expression for the static deflection of the beam:

$$w_\mathrm{b}(x) = F_0 \Upsilon(x - x_\mathrm{F}) - \sum_{i=-N_\mathrm{s}/2}^{N_\mathrm{s}/2} \left( \frac{k_\mathrm{p} k_\mathrm{b}}{k_\mathrm{p} + k_\mathrm{b}} \right) w_\mathrm{b}(il_\mathrm{s}) \Upsilon(x - il_\mathrm{s}), \tag{49}$$

where $\Upsilon(x)$ is defined below:

$$\Upsilon(x) = \left( \frac{\left(\kappa AGx^2 - 6EI\right)x}{12EI\,\kappa AG} \right) \mathrm{sign}(x), \tag{50}$$

in which $\mathrm{sign}(x)$ is the sign function. It must be noted that in Eq. (49) the deflection of the beam at the sleeper locations, i.e. $w_\mathrm{b}(il_\mathrm{s})$, is unknown. To be able to use this equation for obtaining the static deflection of the beam under the static load, $w_\mathrm{b}(il_\mathrm{s})$ must first be found. Eq. (49) is therefore solved $N_\mathrm{s}+1$ times (at $x_i = il_\mathrm{s}$, $i = -N_\mathrm{s}/2, \ldots, N_\mathrm{s}/2$) and the following set of equations in matrix form is obtained:

$$\begin{Bmatrix} w_\mathrm{b}\left(\frac{-N_\mathrm{s}}{2} l_\mathrm{s}\right) \\ w_\mathrm{b}\left(\left(\frac{-N_\mathrm{s}}{2}+1\right) l_\mathrm{s}\right) \\ \vdots \\ w_\mathrm{b}(0) \\ \vdots \\ w_\mathrm{b}\left(\left(\frac{N_\mathrm{s}}{2}-1\right) l_\mathrm{s}\right) \\ w_\mathrm{b}\left(\frac{N_\mathrm{s}}{2} l_\mathrm{s}\right) \end{Bmatrix} = F_0 \begin{bmatrix} \phi_{1,1} & \phi_{1,2} & \cdots & \phi_{1,N_\mathrm{s}+1} \\ \phi_{2,1} & \phi_{2,2} & \cdots & \phi_{2,N_\mathrm{s}+1} \\ \vdots & & \ddots & \vdots \\ \phi_{N_\mathrm{s}+1,1} & \phi_{N_\mathrm{s}+1,2} & \cdots & \phi_{N_\mathrm{s}+1,N_\mathrm{s}+1} \end{bmatrix}^{-1} \begin{Bmatrix} \Upsilon\left(\frac{-N_\mathrm{s}}{2} l_\mathrm{s} - x_\mathrm{F}\right) \\ \Upsilon\left(\left(\frac{-N_\mathrm{s}}{2}+1\right) l_\mathrm{s} - x_\mathrm{F}\right) \\ \vdots \\ \Upsilon(-x_\mathrm{F}) \\ \vdots \\ \Upsilon\left(\left(\frac{N_\mathrm{s}}{2}-1\right) l_\mathrm{s} - x_\mathrm{F}\right) \\ \Upsilon\left(\frac{N_\mathrm{s}}{2} l_\mathrm{s} - x_\mathrm{F}\right) \end{Bmatrix}, \tag{51}$$

where the elements of the matrix $\boldsymbol{\phi}$ are defined as:

$$\phi_{i,j}=\begin{cases}1+\left(\dfrac{k_{\mathrm{p}}k_{\mathrm{b}}}{k_{\mathrm{p}}+k_{\mathrm{b}}}\right)\Upsilon(0) & i=j\\ \left(\dfrac{k_{\mathrm{p}}k_{\mathrm{b}}}{k_{\mathrm{p}}+k_{\mathrm{b}}}\right)\Upsilon\left((i'-j')l_{\mathrm{s}}\right) & i\neq j\end{cases}, \tag{52}$$

in which $i'$and $j'$ are $i-(N_{\mathrm{s}}/2)-1$ and $j-(N_{\mathrm{s}}/2)-1$, respectively. The static deflection of the beam, $w_b(x)$, can be obtained by solving Eq. (51) and substituting the solution into Eq. (49). The static stiffness of the beam may then be calculated as the ratio of the applied static force to the obtained static deflection.

*2.2.3 The dynamic track stiffness*

The dynamic track stiffness can be defined in different ways, see e.g. [12]. Two definitions of this parameter are proposed here and 'tested' in the framework of this paper; (1) the ratio of the static load (half the axle load or wheel load) to the dynamic displacement of the contact point defined in a moving reference system, and (2) the ratio of the contact force (including the static wheel load and dynamic terms) to the dynamic displacement of the contact point defined in a moving reference system. For the wheel/track model developed in this section, the first definition of the dynamic stiffness is mathematically given below:

$$k_{\mathrm{dyn},1}=\frac{F_{\mathrm{axle\,load}}/2}{w_{\mathrm{b}}(x,t=x/v)}. \tag{53}$$

The beam displacement defined in Eq. (33) can be substituted into the latter equation, yielding the dynamic stiffness:

$$k_{\mathrm{dyn},1}=\frac{-\bar{F}_0 v}{\sum_{m=-N_{\mathrm{t}}}^{N_{\mathrm{t}}}\sum_{n=-N_{\mathrm{t}}}^{N_{\mathrm{t}}}(\theta(0))_{m+(N_{\mathrm{t}}+1),n+(N_{\mathrm{t}}+1)}\bar{F}_n\,\mathrm{e}^{\mathrm{j}m(\frac{2\pi}{l_{\mathrm{s}}})x}}. \tag{54}$$

Similarly, the second definition of the dynamic stiffness can be expressed as:

$$k_{\mathrm{dyn},2}=\frac{-v\sum_{m=-\infty}^{+\infty}\bar{F}_m\,\mathrm{e}^{\mathrm{j}m(\frac{2\pi v}{l_{\mathrm{s}}})t}}{\sum_{m=-N_{\mathrm{t}}}^{N_{\mathrm{t}}}\sum_{n=-N_{\mathrm{t}}}^{N_{\mathrm{t}}}(\theta(0))_{m+(N_{\mathrm{t}}+1),n+(N_{\mathrm{t}}+1)}\bar{F}_n\,\mathrm{e}^{\mathrm{j}m(\frac{2\pi}{l_{\mathrm{s}}})x}}. \tag{55}$$

Utilizing the latter equations, it is now possible to calculate minimum and maximum values, and subsequently the amplitude of the variation, for the dynamic stiffness over a certain length of the track. Since the periodic nature of the discrete supports is the only source of non-uniformity for the considered model, these values are obtained over a sleeper bay. In fact, maximum variation of the dynamic stiffness is

normalized with respect to the minimum static stiffness (i.e. the static stiffness calculated at $x = l_s / 2$) and the following parameter is introduced:

$$\left( \frac{\Delta k_{\mathrm{dyn},i}}{k_{\mathrm{st,min}}} \right) \times 100 = \left( \frac{\max(k_{\mathrm{dyn},i}) - \min(k_{\mathrm{dyn},i})}{k_{\mathrm{st}}\big|_{x=l_s/2}} \right) \times 100, \tag{56}$$

where $k_{\mathrm{st,min}}$ can be obtained using the mathematical formulation given in the previous subsection, and $i = 1, 2$ refers to the two definitions of the dynamic stiffness in Eqs. (54) and (55).

## 3 Parametric study of track design and evaluation

In this section, a parametric study is carried out with respect to the effect on energy dissipation in the substructure; afterwards the relation with the proposed engineering parameters (Eqs. (43) and (56)) is explored. The following design and operational variables are taken into consideration: speed of the moving wheel, magnitude of the unsprung mass, rail profile (bending stiffness, shear stiffness and mass), sleeper mass and spacing, rail pad stiffness and damping and ballast stiffness and damping. To each parameter a nominal value is assigned, corresponding to characteristics of typical Dutch track; a lower and an upper limit are assigned as well, so that for all parameters variation within a bandwidth is considered. Nominal values and lower and upper limits are given in Table 1. Moreover, a static wheel load of 100 kN is used; a shear coefficient of 0.34 is assumed for the Timoshenko rail model [36], and the linearized contact stiffness $k_{\mathrm{H}}$ is calculated as $\sqrt[3]{3\times10^{22}\cdot Q}$, where $Q$ is the static wheel load [37]. A convergence study is carried out in order to determine the number of sleepers required for simulations. Obtained results are shown in Fig. 2. It can be seen that the total number of 15 sleepers is sufficient for a reliable calculation of the energy dissipation in the substructure. Moreover, the importance of the beam theory used in the mathematical model is investigated. Obtained results are shown in Fig. 3, showing the dissipated energy in the substructure for both beam models and using nominal values in Table 1. As can be seen, there is a significant difference, particularly at higher speeds for which the Euler model underestimates the dissipated energy. Therefore, the Timoshenko model is employed for the further analysis in this paper.

Table 1. Nominal values and lower and upper limits for the parameters of the model

| Parameters | Lower value | Nominal value | Upper value |
|---|---|---|---|
| **Rail** | | | |
| Bending stiffness ($EI$), MNm$^2$ | - | 4.25 (54E1 profile) | 6.11 (60E1) |
| Mass per length ($\rho A$), kgm$^{-1}$ | - | 54.4 (54E1 profile) | 60.34 (60E1) |
| **Sleeper** | | | |
| Sleeper mass ($M_s$), kg | 50 | 142.5 | 202 |
| Distance between sleepers ($l_s$), m | 0.5 | 0.6 | 0.7 |
| **Pads** | | | |
| Pad stiffness ($k_p$), MNm$^{-1}$ | 30, 200 | 1000 | 1000* |
| Pad damping ($c_p$), kNm$^{-1}$s | 20 | 30 | 1970 |
| **Ballast** | | | |
| Ballast/subgrade stiffness ($k_b$), MNm$^{-1}$ | 40 | 50 | 60 |

| | | | |
|---|---|---|---|
| Ballast/subgrade damping ($c_b$), kNm$^{-1}$s | - | 55 | - |
| **Moving wheel** | | | |
| Speed (km/h) | 0 | - | 300 |
| Unsprung mass (kg) | 600 | 900 | 1200 |

* The pad stiffness in the order of 1000 MN/m corresponds to the Corkelast pad used for typical Dutch track

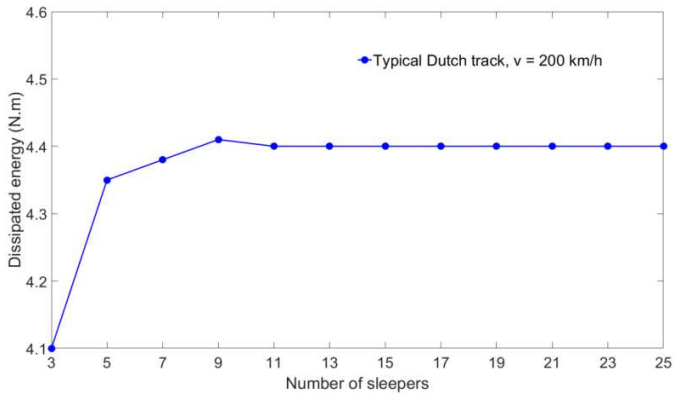


Fig. 2. Model convergence; $v$ = 200 km/h and the nominal values listed in Table 1 have been used for wheel/track parameters

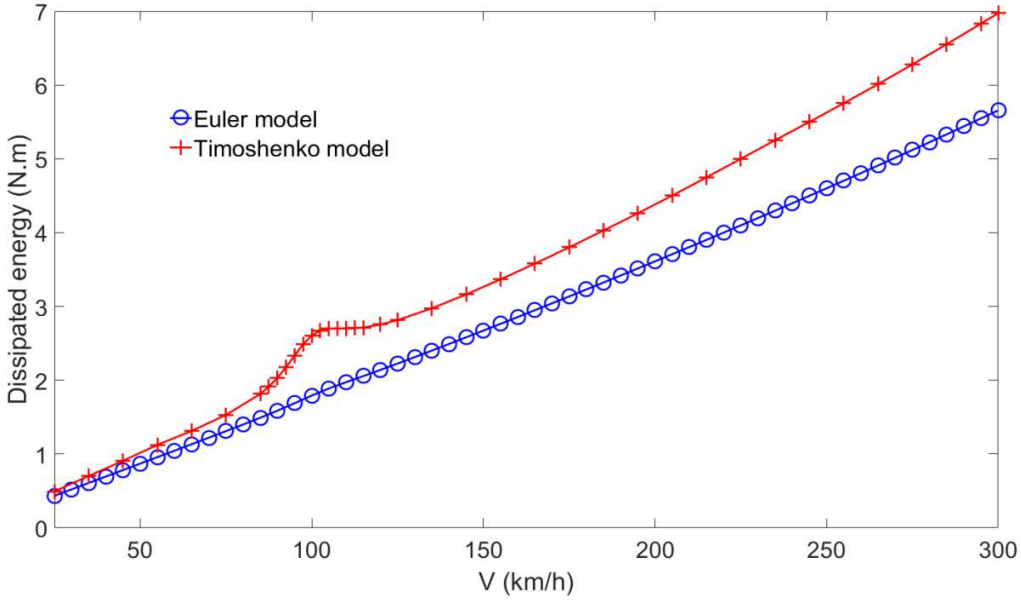


Fig. 3. Dissipated energy calculated using Euler and Timoshenko models; nominal values listed in Table 1 have been used for wheel/track parameters

### *3.1 Wheel/track receptance*

The wheel-track system under consideration can be characterized by its receptance function. Therefore, the response to a unit harmonic force is examined here. In the literature, analytical formulations are available [23, 38, 39], providing information on resonance behavior of railway tracks. However, they do not include a moving wheel. It will be shown that different results are obtained for the receptance including the unsprung vehicle mass, notably in the low-frequency range. In order to find the receptance function for the model, a discretely supported Timoshenko beam coupled to a wheel mass is considered, and response of the beam to a unit harmonic force is obtained utilizing the approach proposed in [40]. According to this approach, discrete supports, and similarly the wheel-beam interaction in this study, are represented by corresponding external forces. Response of the model to all external forces is then obtained employing Green's function of an infinite Timoshenko beam and the superposition principle. A more detailed explanation of the procedure is provided in Appendix A.

Using the nominal values of track parameters given in Table 1 and considering three different values of the unsprung mass, the frequency response of the wheel/track model is obtained and illustrated in Fig. 4. It can be observed that the wheel mass (or, dynamic wheel/track interaction) has a significant influence on the frequency response. In fact, compared to the original track model (solid curve in Fig. 4), the first resonance peak in the frequency response of the rail is shifted to a lower frequency. This is important since it will be shown in the next subsections that the first resonance frequency of the wheel/track model plays a significant role in the analysis of the dynamic stiffness variation of the track and the energy dissipation in the substructure. The presence of the sharp peak available at ~900 Hz in the frequency response of the model (referred to as the 'pinned-pinned frequency') is due to the fact that the response is calculated at midspan. It can be seen that the wheel mass has no significant effect on the pinned-pinned frequency.

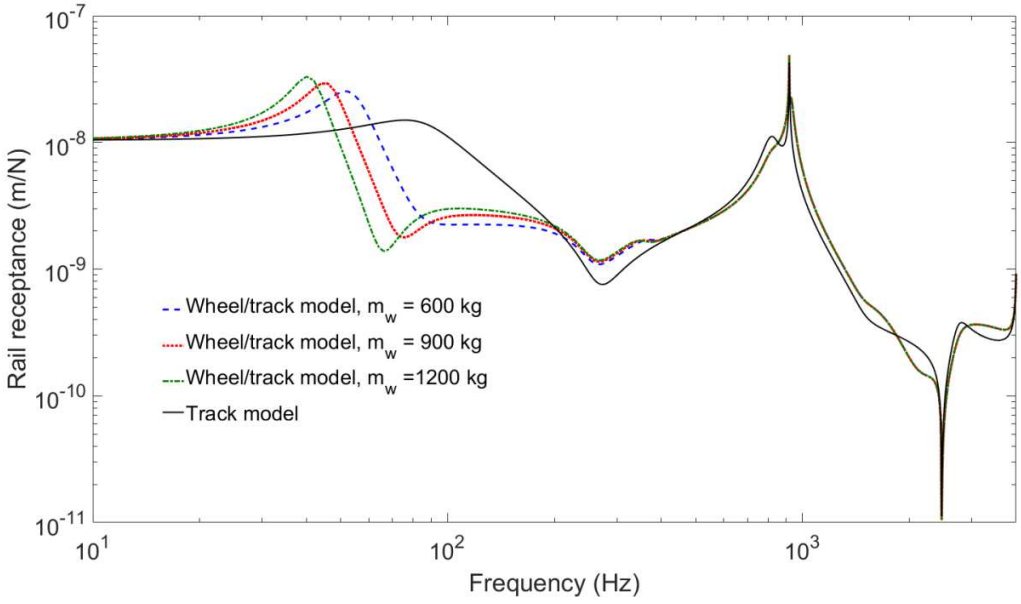

Fig. 4. Amplitude of the wheel/track receptance calculated at midspan

*3.2 Dissipated energy; a parametric study*

This paragraph considers the effect of track design variables on the mechanical energy dissipation in the substructure, considering nominal, minimum and maximum values as listed in Table 1. For the parametric study carried out in this subsection, the dissipated energy in Eq. (43) is normalised with respect to the ballast damping, $c_b$. Results are generally depicted graphically as a function of the train speed.

The effect of the substructure/ballast stiffness is illustrated in Fig. 5 and is significant. For lower values of the ballast/soil stiffness (i.e. soft trackbed foundations), the dissipated energy grows rapidly and rather uniformly with the speed. For an increasingly stiff substructure a different behavior appears, with a much less rapid growth and at the same time a distinct peak in the speed domain. For example, for the ballast stiffness of 200 MN/m, a main peak appears around 155 km/h. This can be explained by the fact that at this speed the sleeper passing frequency (i.e. $v / l_s$) coincides with the first resonance peak in the receptance function of the wheel/track model as discussed in the previous subsection. A second, smaller peak is observed at the speed of 77.5 km/h. This peak can be explained by the presence of multiples of the sleeper passing frequency in the contact force, and the frequency of the second dynamic term, i.e. $\overline{F}_2 \exp\left( j2\pi(2v/l_s)t \right)$, which is close to the first resonance frequency of the wheel/track model. A three-dimensional (3D) plot provides a more comprehensive representation of substructure dissipation in the 2D substructure stiffness – speed domain; such a plot is therefore shown in Fig. 6. From this figure the following conclusions can be drawn with practical relevance: (*i*) the optimum substructure stiffness depends strongly on the operational speed regime; for standard passenger and freight transport a higher stiffness is favorable; (*ii*) the level of mechanical energy, cyclically dissipated in the substructure - and therefore the degradation of high-speed tracks - is higher as compared to conventional lines (roughly with a factor 2 to 3), and (*iii*) the degradation may be very sensitive to particular train velocities, due to resonances in the track receptance. At 300 km/h, subgrade stiffening may reduce the sensitivity to degradation with a factor up to 7-8. It is important to remark that these factors say something about the susceptibility to degradation at the onset of the loading process and may change over the service life, when track unevenness starts to grow and needs to be incorporated in the modeling.

According to the simulation, the dissipated energy grows without any limit as a function of speed. Physically, such unbounded behavior does not make sense. This phenomenon is due to the model adopted in this paper, which is only valid in the subcritical speed domain and cannot be employed for critical or transcritical load speeds, exceeding the Rayleigh wave speed of surface waves. The beam model has a critical velocity equal to the speed of bending/shear waves travelling through the beam, which is much

higher. In the framework of this study, this is not a limitation because of the fact that nearly all trains run at subcritical speeds during daily operation.

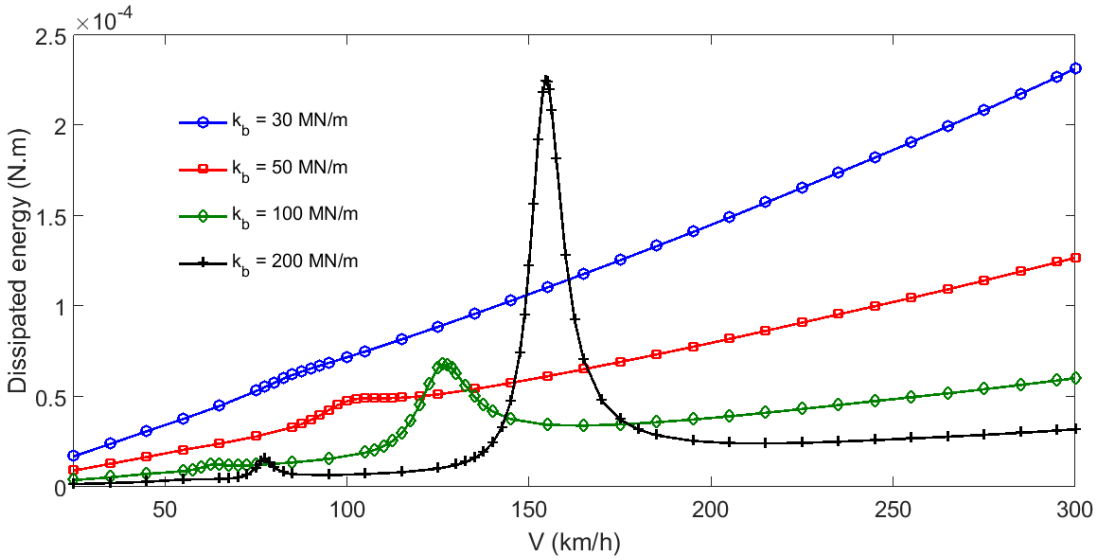


Fig. 5. Effect of ballast/subgrade stiffness on the dissipated energy; unit damping $c_b$, and nominal values for other parameters

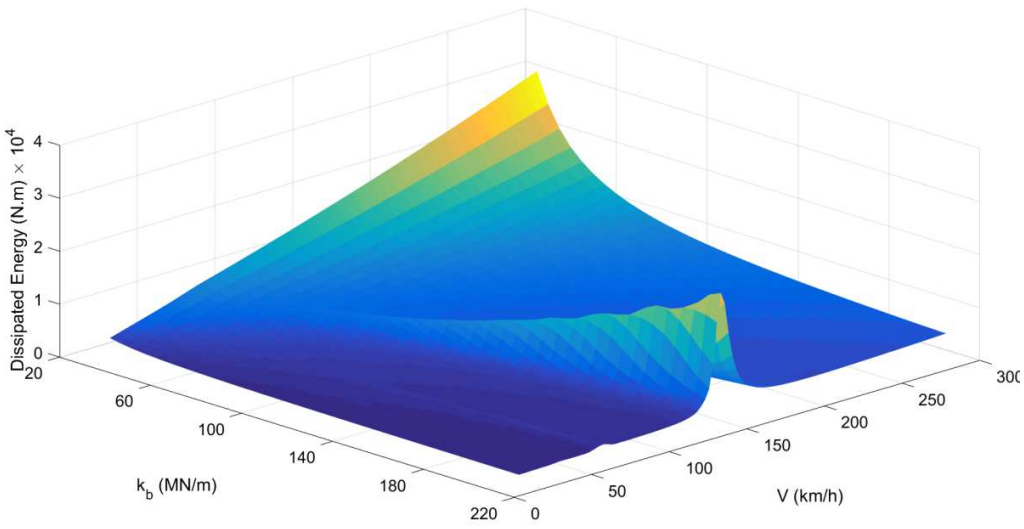


Fig. 6. 3D plot of the dissipated energy for the ballast/subgrade stiffness range 25-205 MN/m; unit damping $c_b$, and nominal values for other parameters

The effect of the railpad stiffness is shown in Fig. 7. The influence of this parameter on the dissipated energy and the long-term degradation is less significant as for the ballast/substructure stiffness; however, degradation increases with the pad stiffness for the entire speed domain. Especially for high-

speed tracks this may become an important parameter, given the cyclic and cumulative effect of dissipation.

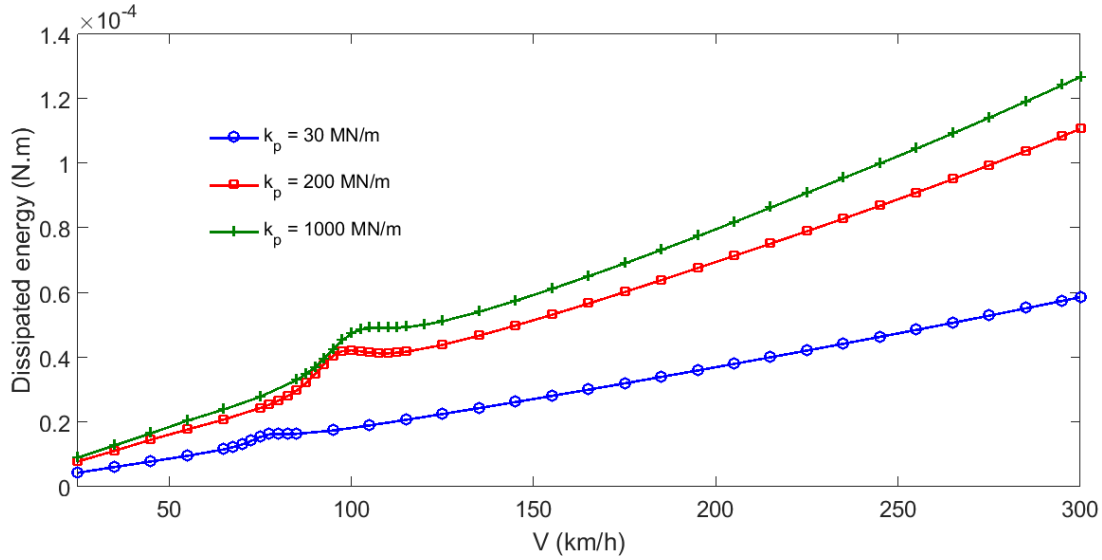


Fig. 7. Effect of pad stiffness on the dissipated energy in the substructure; unit damping $c_b$, and nominal values for other parameters

Fig. 8 shows the influence of the unsprung mass on the energy dissipated in the substructure. It can be concluded that the unsprung mass has a negligible effect on the long-term performance/degradation of the substructure. It should be mentioned here that this conclusion needs to be considered with care and in the framework of this study, which examines the sensitivity of a spatially invariant and geometrically perfect track to degradation. The effect of the unsprung vehicle mass may become significant for spatially variant and irregular track.

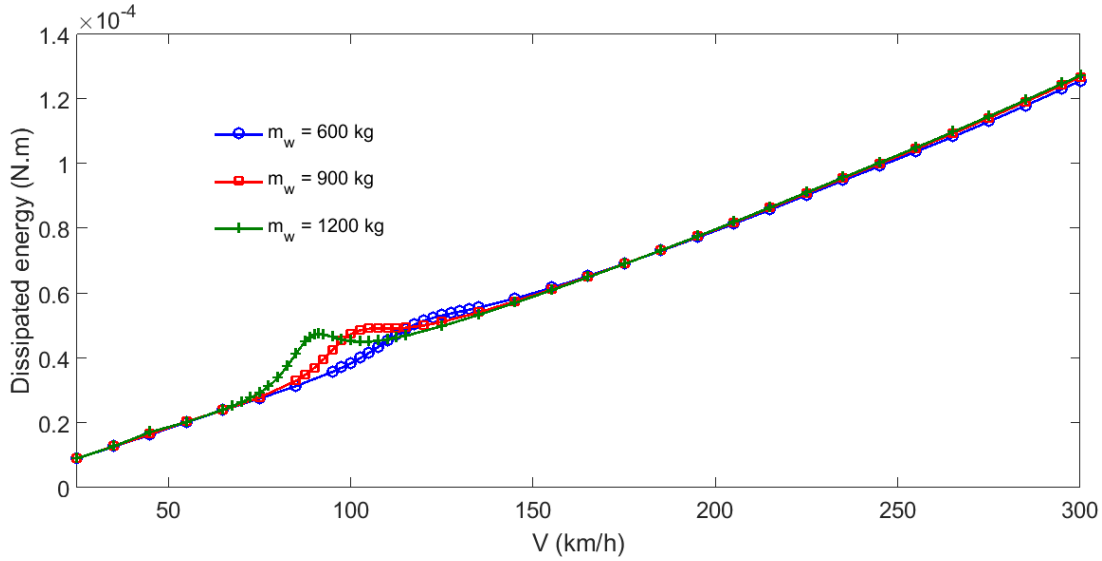

Fig. 8. Effect of unsprung mass on the dissipated energy in the substructure; unit damping $c_b$, and nominal values for other parameters

The influence of the sleeper distance on the dissipated energy is illustrated in Fig. 9. Increasing the distance between sleepers results in a higher rate of degradation for the track for all speeds. Moreover, the importance of the first resonance frequency of the wheel/track model becomes more pronounced for larger values of the sleeper distance.

Fig. 10 and Fig. 11 show the results obtained for different values of sleeper mass and the pad damping, respectively. Although the effect of these parameters becomes more important with increasing speed, they have a negligible influence on the energy dissipated in the substructure. Here, the same remark should be added as for the unsprung mass: the same conclusion is not necessarily valid for spatially variant and irregular track. The effect of the rail profile (cross-sectional properties) is illustrated in Fig. 12, showing that a stiffer rail increases the long-term performance for the entire speed domain.

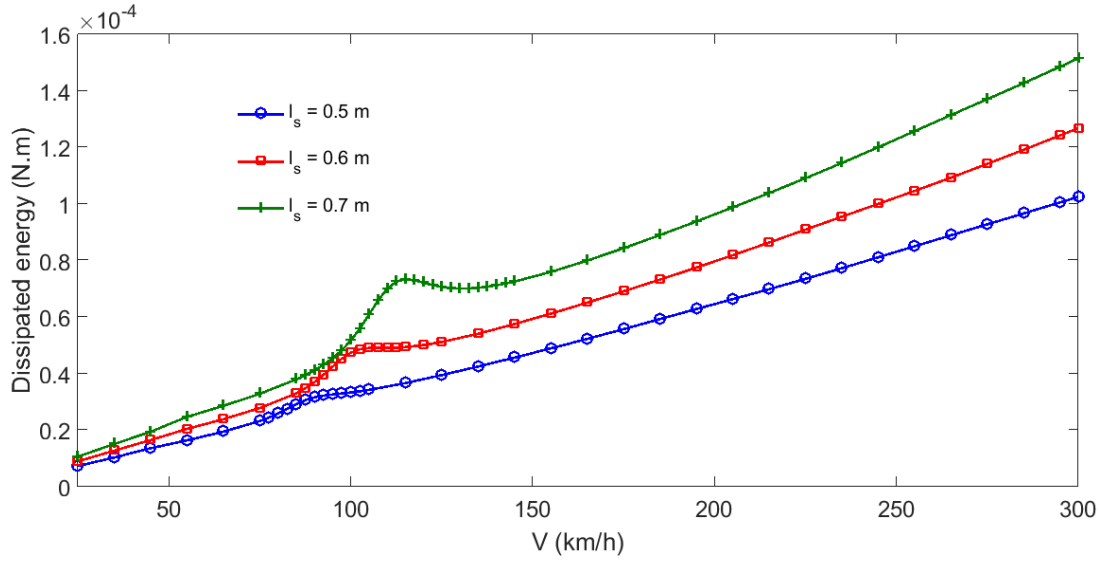


Fig. 9. Effect of sleeper distance on the dissipated energy in the substructure; unit damping $c_b$, and nominal values for other parameters

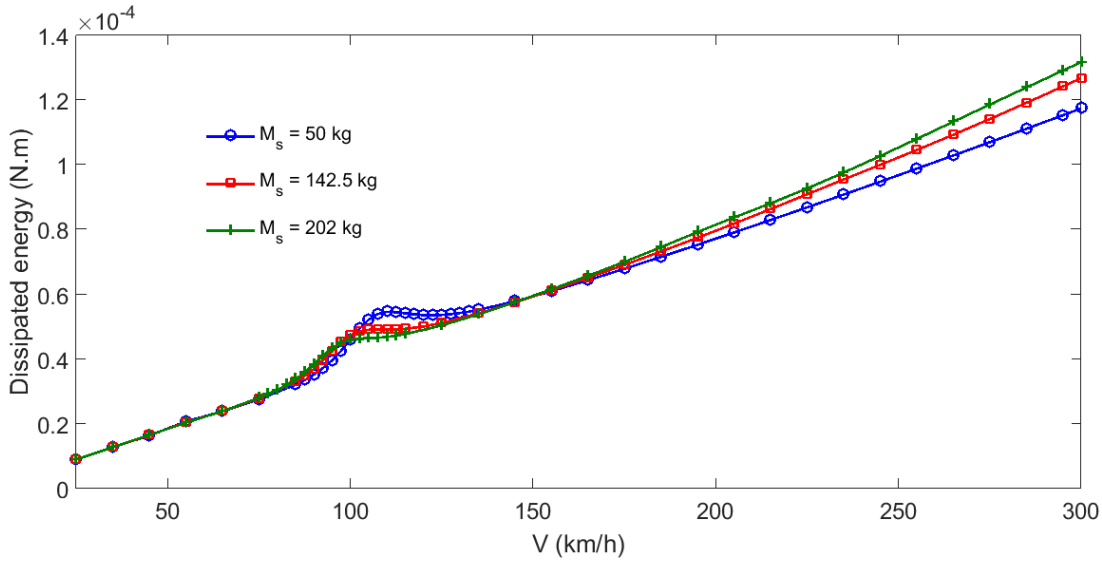


Fig. 10. Effect of sleeper mass on the dissipated energy in the substructure; unit damping $c_b$, and nominal values for other parameters

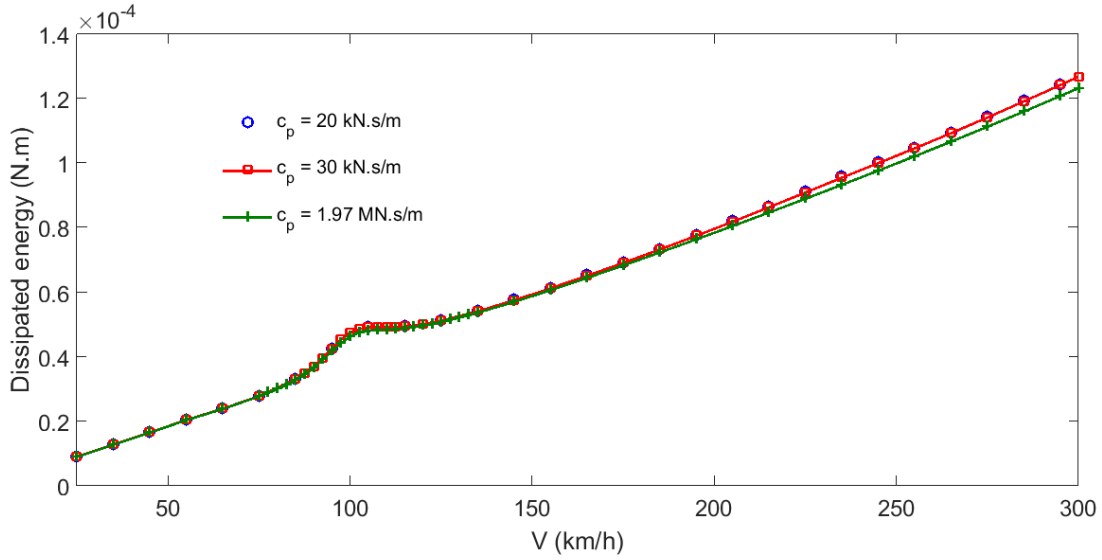


Fig. 11. Effect of the pad damping on the dissipated energy in the substructure; unit damping $c_b$, and nominal values for other parameters

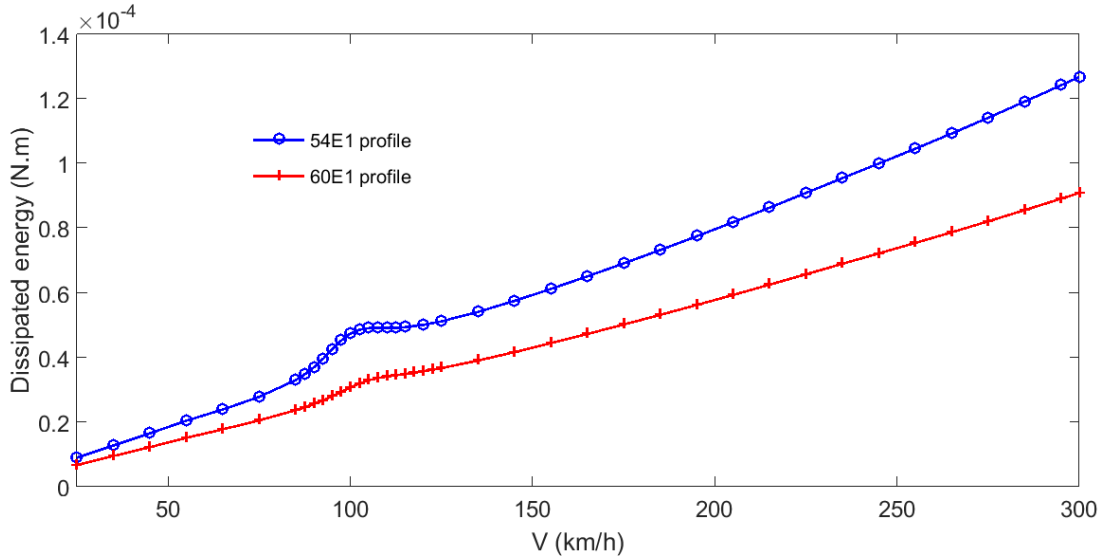


Fig. 12. Effect of rail profile on the dissipated energy in the substructure; unit damping $c_b$, and nominal values for other parameters

In order to allow for a comparison of the relative effect of a variation of different track design parameters at a given train velocity, minimum and maximum values of the dissipation obtained at three practically relevant speeds, $v = 80$, 140 and 250 km/h, are taken from these figures and presented in Table 2. This table allows for an easy comparison of the efficiency of different track design modifications for a given train speed. For example, at 250 km/h, optimizing the ballast/subgrade stiffness is 2.9 times more efficient than optimizing the railpad stiffness. It may be concluded in general that, apart from the operational train speed, the largest effect in the context of sensitivity to degradation can be achieved by adapting the ballast/substructure stiffness; also the railpad stiffness, the sleeper spacing and rail profile can have significant effects, whereas other parameters have a negligible effect – given the assumptions with respect to the track in this study.

Table 2. Minimum and maximum values of the dissipated energy in the substructure (N.m, multiplied by $10^4$) and their difference ($\Delta$) calculated for a single passing axle

| Speed/ Parameters | $k_b$ | | | $k_p$ | | | $l_s$ | | | $m_w$ | | | $M_s$ | | | $c_p$ | | | Rail profile | | |
|---|---|---|---|---|---|---|---|---|---|---|---|---|---|---|---|---|---|---|---|---|---|
| | min | max | Δ | min | max | Δ | min | max | Δ | min | Max | Δ | min | max | Δ | min | max | Δ | min | max | Δ |
| 80 km/h | 0.11 | 0.58 | 0.47 | 0.16 | 0.30 | 0.14 | 0.26 | 0.35 | 0.09 | 0.29 | 0.34 | 0.05 | 0.30 | 0.31 | 0.01 | 0.30 | 0.30 | 0.00 | 0.22 | 0.30 | 0.08 |
| 140 km/h | 0.24 | 0.99 | 0.75 | 0.25 | 0.56 | 0.31 | 0.44 | 0.71 | 0.27 | 0.55 | 0.57 | 0.02 | 0.56 | 0.57 | 0.01 | 0.55 | 0.56 | 0.01 | 0.40 | 0.56 | 0.16 |
| 250 km/h | 0.26 | 1.86 | 1.60 | 0.47 | 1.02 | 0.55 | 0.83 | 1.23 | 0.40 | 1.01 | 1.03 | 0.02 | 0.97 | 1.05 | 0.08 | 0.99 | 1.02 | 0.03 | 0.74 | 1.02 | 0.28 |

*3.3 The dynamic track stiffness; a parametric study*

The dynamic track stiffness is defined as the ratio of the applied force to the dynamic displacement response of the track [12]. For a railway track under a moving axle load, the dynamic track stiffness can also be described as the resistance against deflection experienced in the wheel-rail contact by the moving axle load. As exposed in ref. [3], fluctuations of the dynamic stiffness along the track lead to variations in the wheel/track interaction force. These variations imply a spatial variation of the mechanical energy contained in the moving displacement field, which is partly dissipated in the track, especially at peak fluctuations. Therefore, the dynamic stiffness, and more specifically its spatial variation along the track, is an important and practically relevant parameter that may indicate the track degradation rate. A parametric study is carried out in this subsection, examining the relation between track parameters and the dynamic stiffness. It is important to realise that, given the assumptions of this study, the variation of the dynamic stiffness in the model is exclusively due to the discrete sleeper spacing, whereas practical experience with this parameter [12] is always based on real tracks, with the full range of sources of discontinuity that exist in practice.

Adopting the nominal values, the lower and the upper limits of track parameters listed in Table 1, the non-dimensional definition of the dynamic stiffness variation according to Eq. (56) can be plotted as a function of speed. For the first definition of the dynamic stiffness, the effects of track parameters (except the pad damping which has no significant influence) are illustrated in Fig. 13. The operational speed window, with a lower limit of 80 km/h and an upper limit of 140 km/h, for conventional rail networks has been indicated in this figure using two dashed lines. A critical velocity can be observed with extreme stiffness variation. At this critical velocity, the sleeper passing frequency coincides with the first resonance frequency of the wheel/track model. For speeds exceeding 200 km/h, the stiffness variation is relatively small and becomes nearly independent of speed and other track parameters. It is clear from Fig. 13 that the relationships of substructural energy dissipation and dynamic stiffness variation with the speed are entirely different. The effect of a higher ballast/soil stiffness, leading to a higher stiffness variation and therefore to an assumed higher degradation rate, is predicted incorrectly. At the same time, the effects of increasing railpad stiffness, increasing sleeper spacing, decreasing rail profile stiffness, leading to a higher degradation rate, are correctly predicted, as well as the either negligible or non-unique effects of railpad damping, sleeper mass and unsprung mass. Summarizing, it may be concluded that the dynamic stiffness according to (Eq. (54)) is an inappropriate parameter to predict the sensitivity to degradation, given the model assumptions (track uniformity and straightness) in this study. In other words, this engineering parameter cannot be used at the design stage.

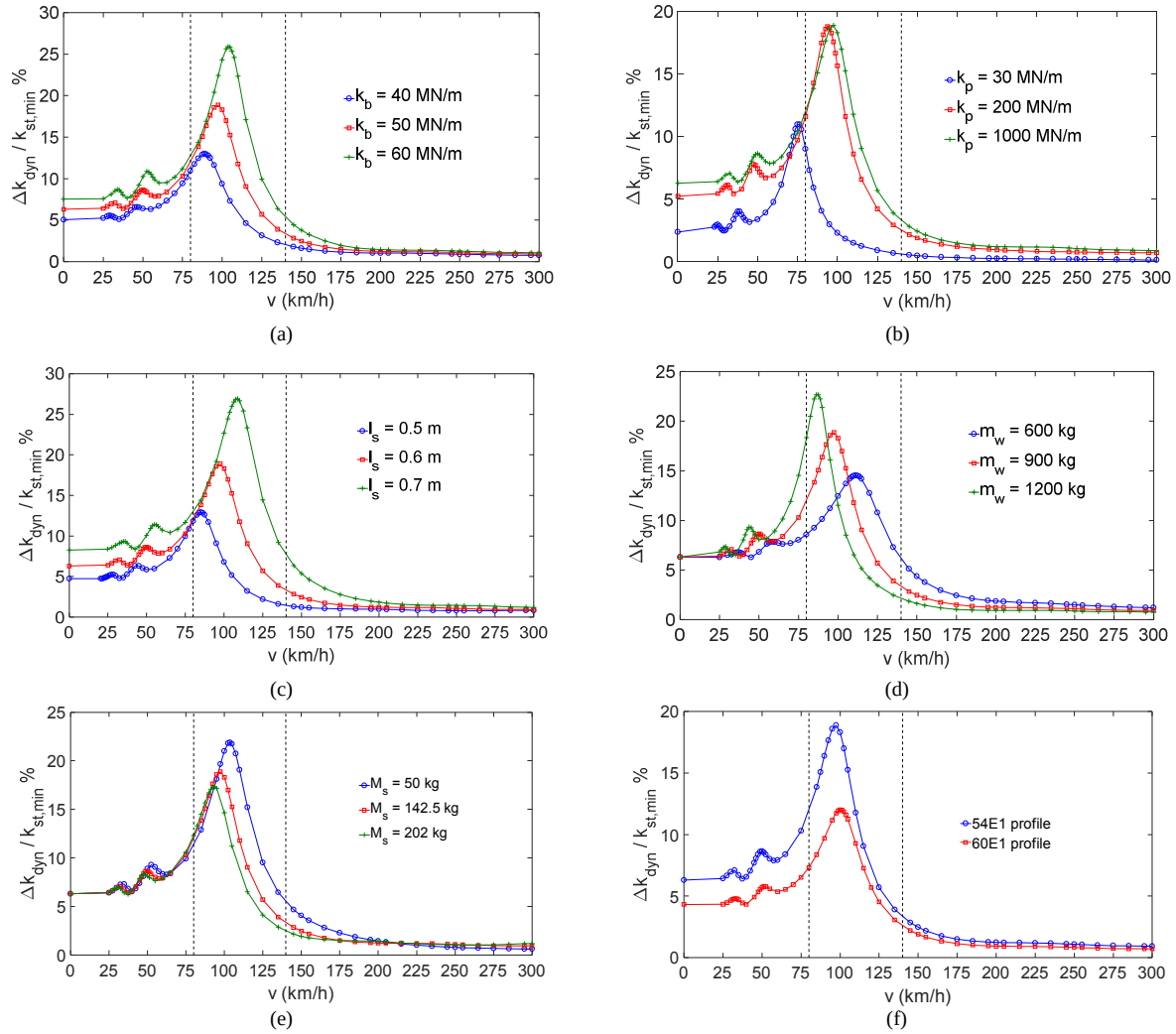


Fig. 13. Effect of different parameters on the first definition (Eq. (54)) of the dynamic stiffness variation; (a) ballast stiffness, (b) pad stiffness, (c) sleeper distance, (d) unsprung mass, (e) sleeper mass and (f) rail profile

Similarly, the effect of track parameters on dynamic stiffness variation is investigated using the second definition in Eq. (55); obtained results are shown in Fig. 14. Compared to the first definition, a different behavior is found as a function of speed, with no peak and the largest magnitude of the variation at the highest speed (300 km/h). Physically, this second definition makes more sense than the first one, as it uses the ratio of the total contact force to the deflection of the contact point. In this case, the dynamic stiffness appears to be dominated by dynamic fluctuations of the contact force, in particular in the high-speed range. Also here, the effect of the ballast/subsoil stiffness is incorrectly predicted, together with other parameters, whereas the effect of other parameters such as the railpad stiffness and the rail profile cross-sectional properties is correctly predicted. It can be concluded that the dynamic track stiffness is inappropriate for assessment of a railway track with respect to long-term behaviour, when this track is idealized assuming invariability of cross-sectional parameters and straightness.

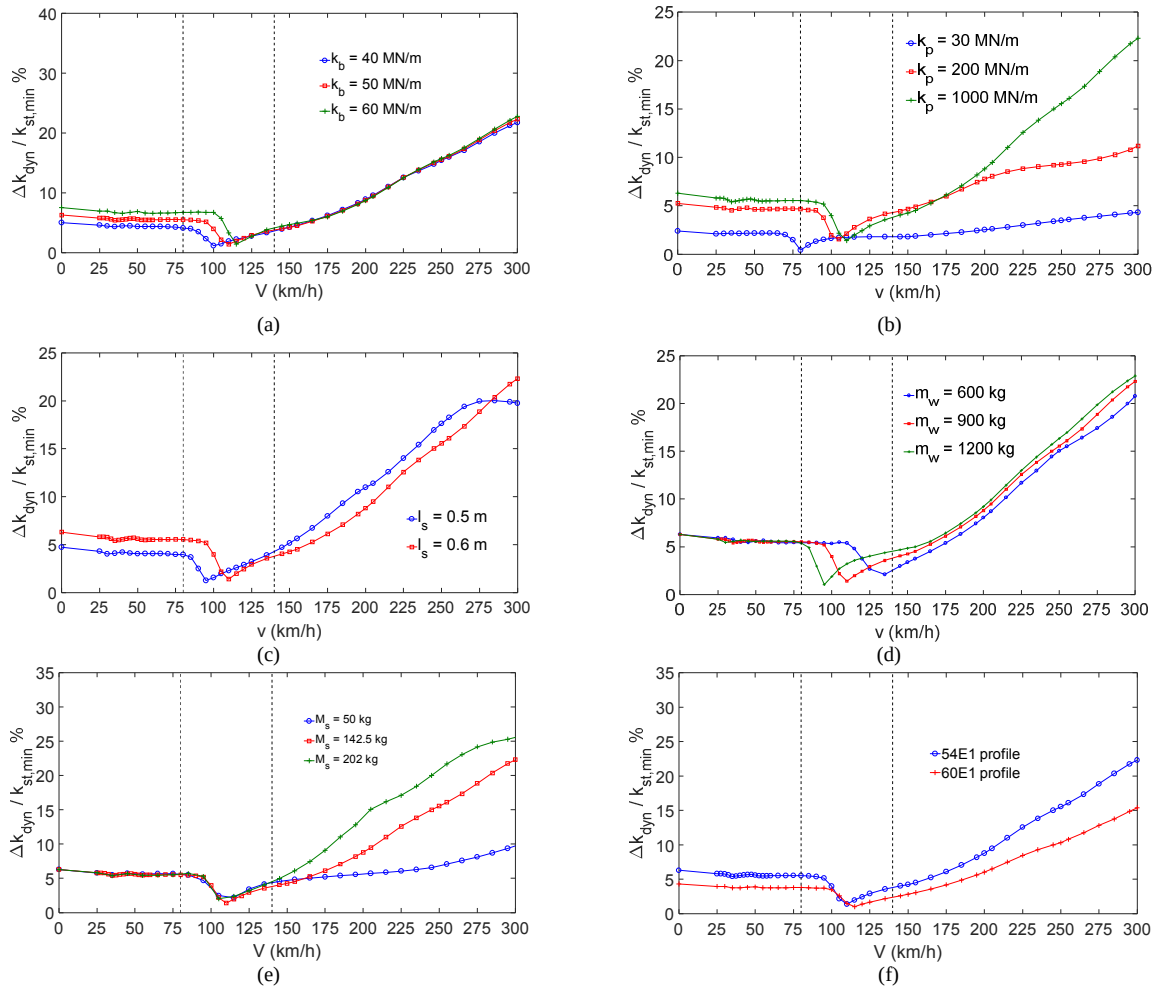


Fig. 14. Effect of different parameters on the second definition (Eq. (55)) of the dynamic stiffness; (a) ballast stiffness, (b) pad stiffness, (c) sleeper distance, (d) unsprung mass, (e) sleeper mass and (f) rail profile

## 4 Conclusions

This paper studied the effect of railway track design parameters on the expected long-term performance, assuming spatial invariability (except for the presence of the discrete sleepers) and geometrical straightness of the track. The susceptibility of the track to degradation was objectively quantified by calculating the mechanical energy dissipated in the substructure under a moving axle load for variations of different track parameters. Hereto, a frequency-domain two-layer model was used of a discretely supported rail coupled with a moving, unsprung mass. The analysis showed that, apart from the operational train speed, the ballast/substructure stiffness is the most significant parameter influencing energy dissipation. Increased degradation rates can therefore be expected for ballasted high-speed lines

with respect to conventional track; the difference is roughly a factor 2 to 3. The difference between very poor and stiff subsoil is roughly a factor 7 to 8 for a high-speed line at 300 km/h; for conventional track, this can be in the same range. However, in the range from 100 – 200 km/h subgrade stiffening is not necessarily a solution, as the dissipation shows localized peaks as a function of the speed with increasing stiffness. These factors say something about the susceptibility to degradation at the onset of the loading process and may change over the service life, when track unevenness starts to grow and needs to be incorporated in the modeling. Also railpad stiffness, sleeper distance and rail profile were found to have considerable effect and therefore to be effective control parameters, with degradation increasing with railpad stiffness, increasing sleeper distance and decreasing rail profile bending stiffness. The unsprung vehicle mass and sleeper mass were found to have no significant influence, however, only against the background of the assumption of a perfect (invariant and straight) track. Apart from dissipated mechanical energy, the suitability of the dynamic track stiffness was explored as an engineering parameter to assess the sensitivity to degradation in the design stage. It was found that this quantity is inappropriate in the case of an idealized track. That leaves the possibility open that the parameter works well, even theoretically, for realistic tracks including the full range of possibilities for spatial variation of cross-sectional properties that exist in practice.

## 5. Acknowledgements

The present study makes part of a long-term and wider-scope project aiming at an improved understanding of the physics of track degradation and environmental vibration radiation due to train operation. This project is executed by Delft University of Technology with financial support from the Dutch rail infra manager ProRail. The authors want to thank especially Arjen Zoeteman from ProRail for his strong motivation and support to make scientific work in this domain possible.

## Appendix A. Receptance of a discretely supported Timoshenko beam coupled with an oscillator

In this appendix a mathematical formulation is derived of the receptance of an infinite Timoshenko beam with discrete supports, coupled with a stationary wheel mass. A schematic overview of the model is shown in Fig. 1; the only difference is that, instead of a moving wheel, a stationary wheel is considered here and that the model is excited by a harmonic force of amplitude $F_0$, at $x = x_F$. The response of an infinite Timoshenko beam to a unit harmonic force at $x = x'$, i.e. the Green's function, $G(x, x')$, is given as [41]:

$$G(x, x') = u_1 e^{-jk_1|x-x'|} + u_2 e^{-k_2|x-x'|}, \tag{A.1}$$

where $k_1$ and $k_2$ are complex wavenumbers defined as follows:

$$k_1 = \frac{\omega}{\sqrt{2}}\sqrt{\rho\left(\frac{1}{E}+\frac{1}{\kappa G}\right)+\sqrt{\left(\frac{\rho}{E}-\frac{\rho}{\kappa G}\right)^2+\frac{4\rho A}{EI\omega^2}}}, \tag{A.2}$$

$$k_2 = \frac{\omega}{\sqrt{2}}\sqrt{-\rho\left(\frac{1}{E}+\frac{1}{\kappa G}\right)+\sqrt{\left(\frac{\rho}{E}-\frac{\rho}{\kappa G}\right)^2+\frac{4\rho A}{EI\omega^2}}}. \tag{A.3}$$

Moreover, $u_1$ and $u_2$ are given by:

$$u_1 = \frac{\mathrm{j}}{\kappa GEI}\frac{\rho I\omega^2-\kappa GA-EIk_1^{\,2}}{2Ak_1\left(k_1^{\,2}+k_2^{\,2}\right)}, \tag{A.4}$$

$$u_2 = \frac{1}{\kappa GEI}\frac{\rho I\omega^2-\kappa GA+EIk_2^{\,2}}{2Ak_2\left(k_1^{\,2}+k_2^{\,2}\right)}. \tag{A.5}$$

The discrete supports and the wheel-track coupling can be replaced by corresponding external forces, and the total response of the Timoshenko beam at any arbitrary point *x* can be found using the Green's function defined in (A.1) and the superposition principle:

$$\bar{W}_{\mathrm{b}}(x) = F_0 G(x,x_{\mathrm{F}}) - \left(\sum_{i=-N_{\mathrm{s}}/2}^{N_{\mathrm{s}}/2} Z_{\mathrm{s}}\bar{W}_{\mathrm{b}}(il_{\mathrm{s}})G(x,il_{\mathrm{s}})\right) + Z_{\mathrm{w}}\bar{W}_{\mathrm{b}}(0)G(x,0), \tag{A.6}$$

where $Z_{\mathrm{s}}$ and $Z_{\mathrm{w}}$ are the dynamic stiffness caused by the supports and the wheel, respectively. The last term in the latter equation is added to the total response of the infinite Timoshenko beam with discrete supports available in the literature, in order to include the track-wheel coupling and investigate its influence on frequency response of railway track. The following analytical expressions can be derived for $Z_{\mathrm{s}}$ and $Z_{\mathrm{w}}$:

$$Z_{\mathrm{s}} = \frac{\left(k_{\mathrm{p}}+\mathrm{j}\omega c_{\mathrm{p}}\right)\left(-M_{\mathrm{s}}\omega^2+\mathrm{j}\omega c_{\mathrm{b}}+k_{\mathrm{b}}\right)}{-M_{\mathrm{s}}\omega^2+\mathrm{j}\omega\left(c_{\mathrm{p}}+c_{\mathrm{b}}\right)+\left(k_{\mathrm{p}}+k_{\mathrm{b}}\right)}, \tag{A.7}$$

$$Z_{\mathrm{w}} = \frac{k_{\mathrm{H}}m_{\mathrm{w}}\omega^2}{k_{\mathrm{H}}-m_{\mathrm{w}}\omega^2}. \tag{A.8}$$

It must be noted that the right-hand side of (A.6) contains the unknown response of the model at supports locations. Therefore, in order to be able to obtain the response at any arbitrary location along the track by utilizing this equation, the unknown response of the system at the support locations must be found first. This can be carried out by setting $x = il_{\mathrm{s}},\ i = -N_{\mathrm{s}}/2,...,N_{\mathrm{s}}/2$, in (A.6), generating $N_{\mathrm{s}}$+1 linear equations and solving the system of equations.

**References**

[1] C. Esveld, C. Esveld, Modern railway track, MRT-productions Zaltbommel, The Netherlands, 2001.

[2] M. Steenbergen, E. de Jong, Railway track degradation: The contribution of rolling stock, Proceedings of the Institution of Mechanical Engineers, Part F: Journal of Rail and Rapid Transit, 230 (2016) 1164-1171.
[3] M.J.M.M. Steenbergen, Physics of railroad degradation: The role of a varying dynamic stiffness and transition radiation processes, Computers & Structures, 124 (2013) 102-111.
[4] M. Brough, A. Stirling, G. Ghataora, K. Madelin, Evaluation of railway trackbed and formation: a case study, NDT & E International, 36 (2003) 145-156.
[5] T. Dahlberg, Some railroad settlement models—a critical review, Proceedings of the Institution of Mechanical Engineers, Part F: Journal of Rail and Rapid Transit, 215 (2001) 289-300.
[6] Y. Sato, Japanese studies on deterioration of ballasted track, Vehicle system dynamics, 24 (1995) 197-208.
[7] N. Lyngby, Railway Track Degradation: Shape and Influencing Factors, International Journal of Performability Engineering, 5 (2009).
[8] J. Sadeghi, H. Askarinejad, Influences of track structure, geometry and traffic parameters on railway deterioration, International Journal of Engineering, Transactions B: Applications, 20 (2007) 292-300.
[9] J.N. Varandas, P. Hölscher, M.A. Silva, Settlement of ballasted track under traffic loading: application to transition zones, Proceedings of the Institution of Mechanical Engineers, Part F: Journal of Rail and Rapid Transit, 228 (2014) 242-259.
[10] T. Abadi, L. Le Pen, A. Zervos, W. Powrie, A Review and Evaluation of Ballast Settlement Models using Results from the Southampton Railway Testing Facility (SRTF), Procedia Engineering, 143 (2016) 999-1006.
[11] I. Soleimanmeigouni, A. Ahmadi, U. Kumar, Track geometry degradation and maintenance modelling: A review, Proceedings of the Institution of Mechanical Engineers, Part F: Journal of Rail and Rapid Transit, (2016) 0954409716657849.
[12] E.G. Berggren, Railway track stiffness: dynamic measurements and evaluation for efficient maintenance, in, KTH, 2009.
[13] E.G. Berggren, A. Nissen, B.S. Paulsson, Track deflection and stiffness measurements from a track recording car, Proceedings of the Institution of Mechanical Engineers, Part F: Journal of Rail and Rapid Transit, 228 (2014) 570-580.
[14] A. Lundqvist, T. Dahlberg, Railway track stiffness variation-consequences and countermeasures, in: 19th IAVSD Symposium of Dynamics of Vehicles on Roads and Tracks, Milano, August 29-Seprember 2, 2005, Dept Mech Eng, Politecnico di Milano, 2005.
[15] E.G. Berggren, A.M. Kaynia, B. Dehlbom, Identification of substructure properties of railway tracks by dynamic stiffness measurements and simulations, Journal of Sound and Vibration, 329 (2010) 3999-4016.
[16] A.V. Metrikine, A. Bodare, Identification of effective properties of the railway substructure in the low-frequency range using a heavy oscillating unit on the track, Archive of Applied Mechanics, 80 (2010) 959-968.
[17] H. Luomala, A. Nurmikolu, Railway track stiffness measurements at bridge transition zones, Advances in Transportation Geotechnics 2, (2012) 161.
[18] P. Belotserkovskiy, On the oscillations of infinite periodic beams subjected to a moving concentrated force, Journal of Sound and Vibration, 193 (1996) 705-712.
[19] S. Lu, D. Xuejun, Dynamic analysis to infinite beam under a moving line load with uniform velocity, Applied mathematics and mechanics, 19 (1998) 367-373.
[20] L. Sun, A closed-form solution of beam on viscoelastic subgrade subjected to moving loads, Computers & structures, 80 (2002) 1-8.
[21] L. Sun, F. Luo, Steady-state dynamic response of a Bernoulli–Euler beam on a viscoelastic foundation subject to a platoon of moving dynamic loads, Journal of Vibration and Acoustics, 130 (2008) 051002.

[22] S. Koroma, M. Hussein, J. Owen, Vibration of a beam on continuous elastic foundation with nonhomogeneous stiffness and damping under a harmonically excited mass, Journal of Sound and Vibration, 333 (2014) 2571-2587.
[23] S. Grassie, R. Gregory, D. Harrison, K. Johnson, The dynamic response of railway track to high frequency vertical excitation, Journal of Mechanical Engineering Science, 24 (1982) 77-90.
[24] J. Kalker, Discretely supported rails subjected to transient loads, Vehicle System Dynamics, 25 (1996) 71-88.
[25] I. Zobory, V. Zoller, Dynamic response of a periodically supported railway track in case of a moving complex phasor excitation, in: Progress in Industrial Mathematics at ECMI 96, Springer, 1997, pp. 85-92.
[26] P. Belotserkovskiy, Forced oscillations of infinite periodic structures. Applications to railway track dynamics, Vehicle System Dynamics, 29 (1998) 85-103.
[27] M. Shamalta, A.V. Metrikine, Analytical study of the dynamic response of an embedded railway track to a moving load, Archive of Applied Mechanics, 73 (2003) 131-146.
[28] T. Hoang, D. Duhamel, G. Foret, H. Yin, P. Joyez, R. Caby, Calculation of force distribution for a periodically supported beam subjected to moving loads, Journal of Sound and Vibration, 388 (2017) 327-338.
[29] A.V. Metrikine, K. Popp, Vibration of a periodically supported beam on an elastic half-space, European Journal of Mechanics-A/Solids, 18 (1999) 679-701.
[30] A. Vostroukhov, A. Metrikine, Periodically supported beam on a visco-elastic layer as a model for dynamic analysis of a high-speed railway track, International Journal of Solids and Structures, 40 (2003) 5723-5752.
[31] X. Sheng, C. Jones, M. Petyt, Ground vibration generated by a load moving along a railway track, Journal of sound and vibration, 228 (1999) 129-156.
[32] G. Lombaert, G. Degrande, J. Kogut, S. François, The experimental validation of a numerical model for the prediction of railway induced vibrations, Journal of Sound and Vibration, 297 (2006) 512-535.
[33] M.J.M.M. Steenbergen, A.V. Metrikine, The effect of the interface conditions on the dynamic response of a beam on a half-space to a moving load, European Journal of Mechanics-A/Solids, 26 (2007) 33-54.
[34] G. Kouroussis, D.P. Connolly, O. Verlinden, Railway-induced ground vibrations–a review of vehicle effects, International Journal of Rail Transportation, 2 (2014) 69-110.
[35] J.C. Nielsen, J. Oscarsson, Simulation of dynamic train–track interaction with state-dependent track properties, Journal of sound and vibration, 275 (2004) 515-532.
[36] M.J.M.M. Steenbergen, H. de Graaf, On the effect of wheel flat wear on dynamic wheel-rail interaction force levels, in: The international conference on bogies, Budapest, Hungary, 2013, pp. 9-12.
[37] M.J.M.M. Steenbergen, Modelling of wheels and rail discontinuities in dynamic wheel–rail contact analysis, Vehicle System Dynamics, 44 (2006) 763-787.
[38] D.J. Thompson, N. Vincent, Track dynamic behaviour at high frequencies. Part 1: theoretical models and laboratory measurements, Vehicle System Dynamics, 24 (1995) 86-99.
[39] A. Nordborg, Vertical rail vibrations: Pointforce excitation, Acta Acustica united with Acustica, 84 (1998) 280-288.
[40] M.A. Heckl, Railway noise–Can random sleeper spacings help?, Acta Acustica united with Acustica, 81 (1995) 559-564.
[41] T. Wu, D.J. Thompson, The effects of local preload on the foundation stiffness and vertical vibration of railway track, Journal of Sound and Vibration, 219 (1999) 881-904.